Instituto de Física de Cantabria

CMB and non-Gaussianity

Enrique Martínez-González
Instituto de Física de Cantabria
Santander (Spain)

International School of Astroparticle Physics, La Palma, July 2012

Outline

- Beyond the power spectrum
- Inflation model
- Isotropy and Gaussianity:
  - Non-standard inflationary models
  - Topological defects
  - Geometry and topology
  - Primordial magnetic fields
- Secondary anisotropies and contaminants:
  - Combined ISW-lensing effect
  - Extragalactic sources
- Summary

Isotropic Gaussian Random Field

- Definition of a Gaussian Random Field $y(\vec{r})$:
  - For any set of n points $\vec{r}_1, \vec{r}_2, \ldots, \vec{r}_n$ the n-point probability density function of the random field on those points $y_1, y_2, \ldots, y_n$ is an n-point multinomial distribution:

$$f(y_1, y_2, \ldots, y_n) = \frac{1}{(2\pi)^{n/2}|M|^{1/2}} \exp \sum_{ij} (y_i - \bar{y}_i) M_{ij}^{-1} (y_j - \bar{y}_j)$$

where $M_{ij} = \langle (y_i - \bar{y}_i)(y_j - \bar{y}_j) \rangle$. In the case of the CMB anisotropies, the support is the sphere and the points are directions on the sky.

- Statistical isotropy:
  - The CMB anisotropies are said to be statistically isotropic if for any pair of points:

$$\langle y(\vec{r}_1) y(\vec{r}_2) \rangle = C(|\vec{r}_1 - \vec{r}_2|)$$

Temperature anisotropies

- The CMB temperature anisotropies can be decomposed in terms of the spherical harmonic coefficients:

$$\frac{\Delta T}{T}\left(\vec{n}\right) = a^{T}_{\ell m} Y_{\ell m}\left(\vec{n}\right)$$

- An important statistical quantity is the CMB (rotationally invariant) power spectrum which is defined as:

$$C_{\ell} = \left\langle \left| a^{T}_{\ell m} \right|^{2} \right\rangle \quad \text{and it is estimated from a map as} \quad C_{\ell} = \frac{1}{2\ell+1} \sum_{m} \left| a^{T}_{\ell m} \right|^{2}$$

- For polarization the Q,U Stokes parameters are usually transformed in the scalar quantities E,B modes as follows:

$$\left(Q + iU\right)\left(\vec{n}\right) = \sum_{\ell,m} a^{(\pm 2)}_{\ell m}\, {}_{\pm 2}Y_{\ell m}\left(\vec{n}\right)$$

$$a^{E}_{\ell m} \equiv -\frac{1}{2}\left(a^{(2)}_{\ell m} + a^{(-2)}_{\ell m}\right), a^{B}_{\ell m} \equiv -\frac{1}{2i}\left(a^{(2)}_{\ell m} - a^{(-2)}_{\ell m}\right)$$

$$E\left(\vec{n}\right) = \sum_{\ell m} a^{E}_{\ell m} Y_{\ell m}\left(\vec{n}\right), B\left(\vec{n}\right) = \sum_{\ell m} a^{B}_{\ell m} Y_{\ell m}\left(\vec{n}\right)$$

Cosmic Variance

The power spectrum C_l and the correlation function $C(\theta)$ are related by the Legendre transformation:

$$C(\theta) \equiv \left\langle \frac{\Delta T}{T}(\vec{n}_1)\frac{\Delta T}{T}(\vec{n}_2) \right\rangle = \sum_l \frac{2l+1}{4\pi} C_l P_l(\cos\theta)$$

where $$C_l \equiv \frac{1}{2l+1}\sum_{m=-l}^{l} |\, a_{lm}\,|^2$$

For an IGRF it is possible to get the variance of the power spectrum C_l in an analytical form:

$$\Delta C_l = \frac{1}{\sqrt{l+0.5}} C_l$$

This is the dispersion of a χ^2 distribution with 2l+1 dof.

CMB science:
C_l information

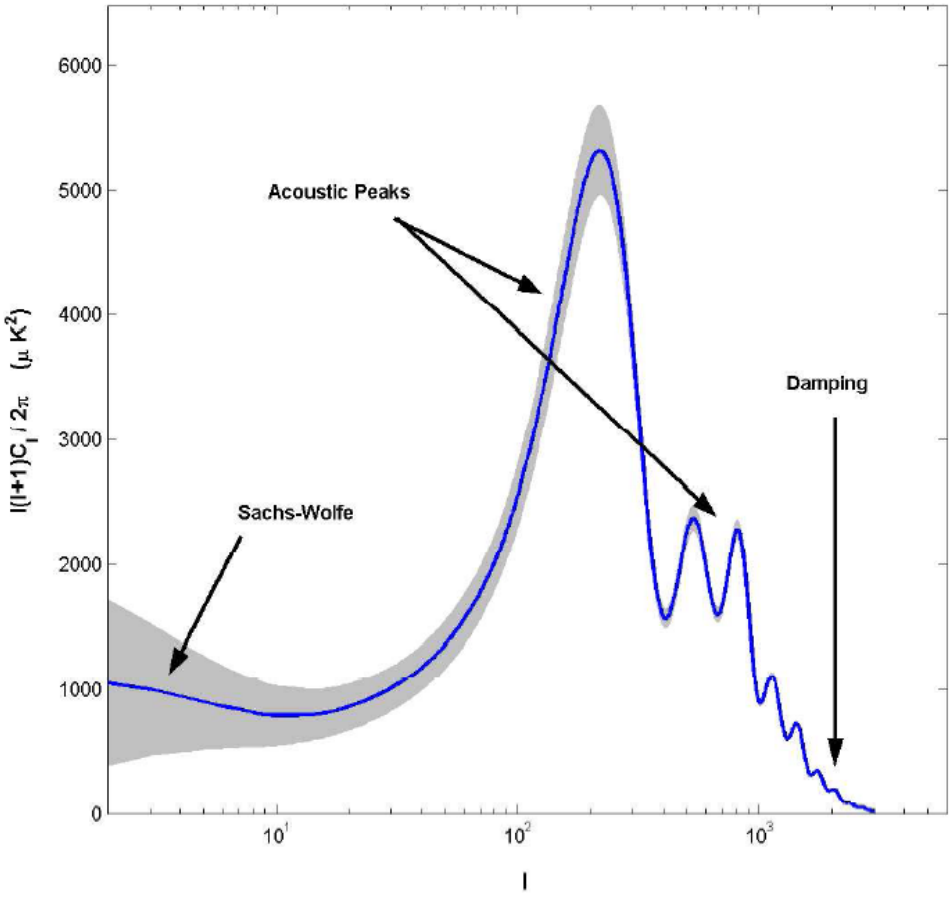

Planck will provide a nearly cosmic-variance-limited C_l in the multipole range $2 < l < 2000$ where primary anisotropies dominate.

The CMB represents a unique observation to understand the universe

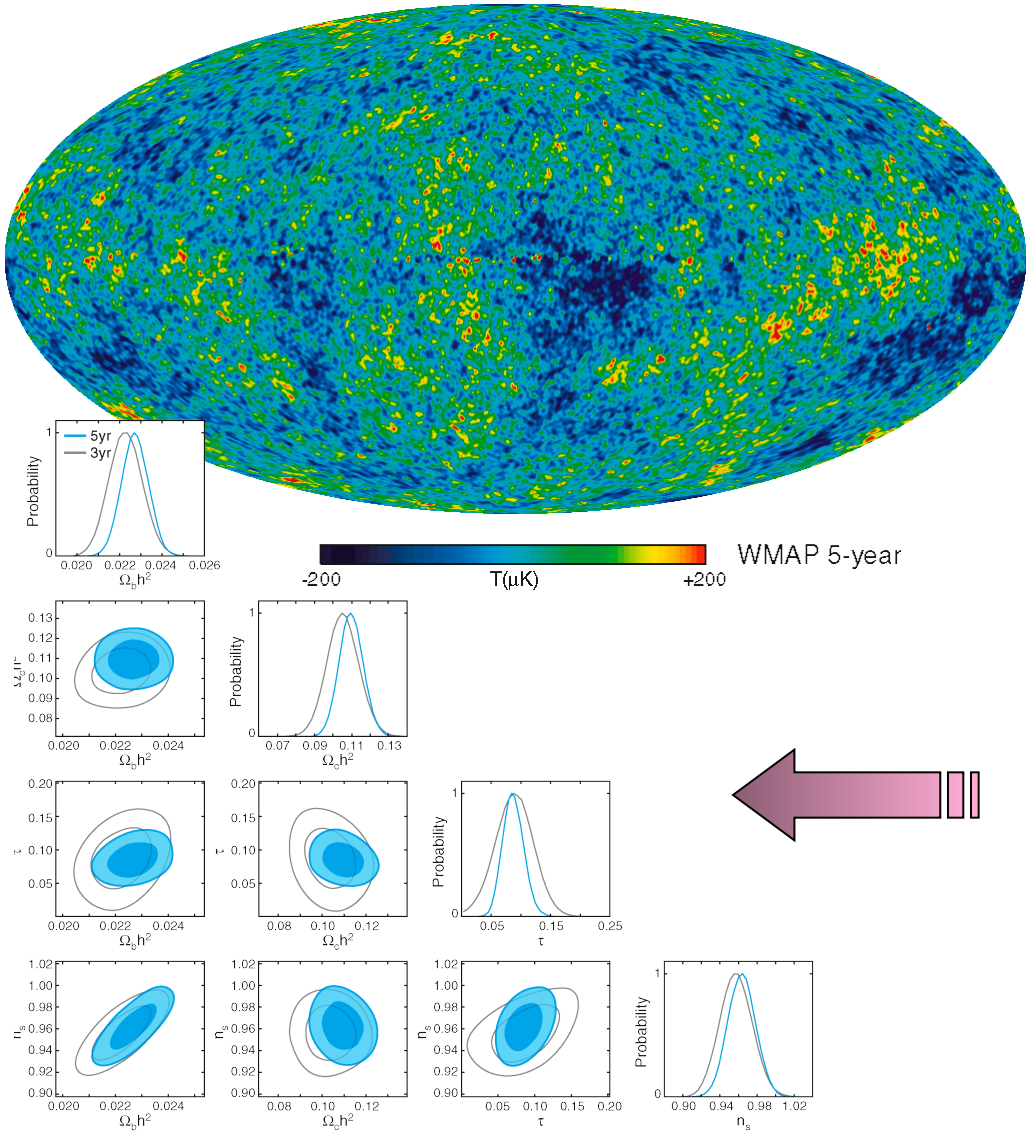

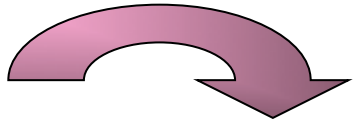

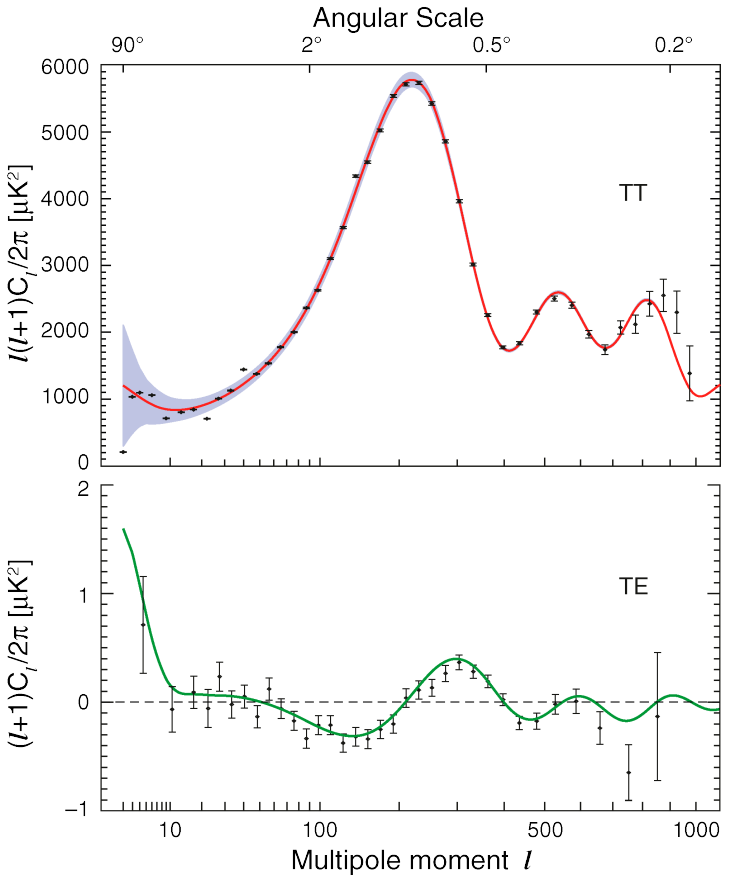

The power spectrum and beyond

- Two fundamental properties of the cosmological paradigm are the homogeneity and isotropy of the matter-energy content of the universe and the Gaussianity of the initial perturbations.
- Those fundamental properties can be tested with precise observations of the CMB anisotropies. Due to the linear processes involved in the generation of those anisotropies the CMB test is straightforward. Cosmological studies based on e.g. the galaxy distribution or gravitational lensing are complicated by non-linear fenomena, as gravitational collapse or the bias, …
- Under the assumption of Gaussianity and isotropy all the information is contained in the power spectrum of the CMB anisotropies.
- Testing Gaussianity and isotropy is important because:
  - It justifies the assumptions made in the process of deriving the cosmological parameters from the power spectrum.
  - It probes new physics and new scenarios of the early universe and of the geometry of the universe.
  - It allows a better understanding of secondary fenomena giving rise to deviations from Gaussianity.

Inflationary paradigm

Condition for accelerated expansion: $\rho + 3p < 0$

Single scalar field: $\rho_\phi = \frac{1}{2}\left(\frac{d\phi}{dt}\right)^2 + V(\phi) \qquad p_\phi = \frac{1}{2}\left(\frac{d\phi}{dt}\right)^2 - V(\phi)$

$\left(\frac{d\phi}{dt}\right)^2 < V(\phi) \longrightarrow$ Accelerated expansion: $a(t) \approx a_0 \exp[H(t - t_0)]$

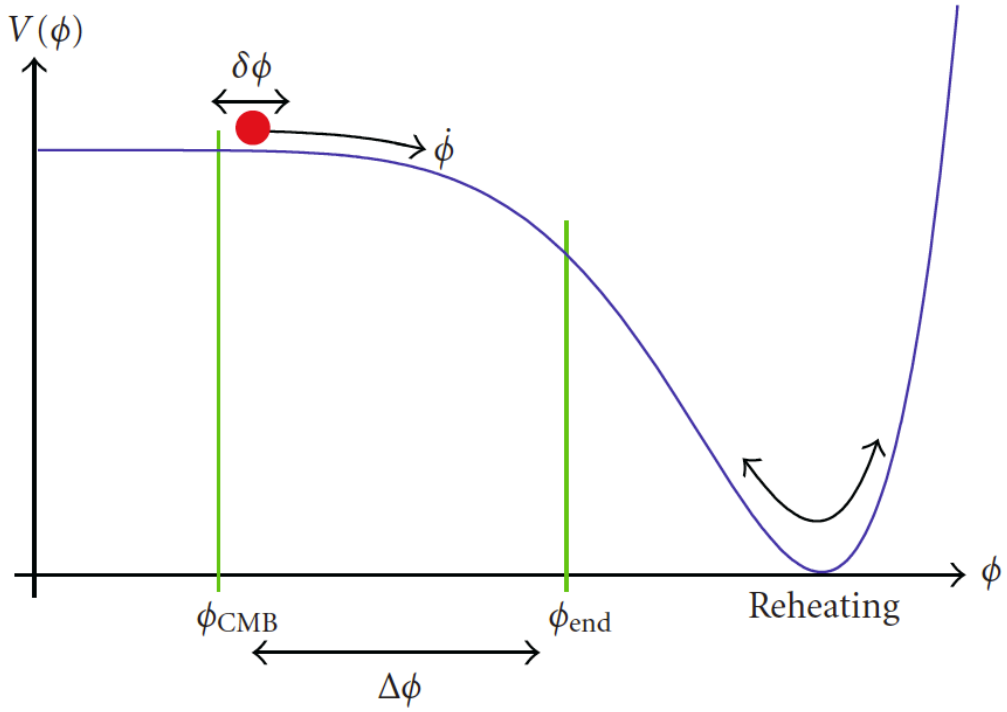

CONNECTION BETWEEN INFLATIONARY PARAMETERS AND OBSERVATIONS

- The slow-roll parameters of inflation are connected to observations as:

  - Fluctuation spectrum: $\Delta = Ak^n$

  - $n_s = 1 - 6\varepsilon + 2\eta \approx 1$
  - $n_t = -2\varepsilon$
  - $r \equiv \frac{A_t^2}{A_s^2} = 16\varepsilon$

$$\varepsilon = \frac{M_p^2}{2}\left(\frac{V'}{V}\right)^2$$

$$\eta = M_p^2\left(\frac{V''}{V}\right)$$

PREDICTIONS FROM INFLATION

- Generation of the initial energy-density fluctuations of the adiabatic type
- Nearly scale-invariant spectrum of fluctuations: scalar spectral index $n_s \leq 1$ (0.92-0.98)
- Generation of the Gravitational Wave Background $\Rightarrow$ existence of B-mode polarization

From WMAP and LSS: $n_s \approx 0.96 \Rightarrow 3\varepsilon - \mu \approx 0.02$

$$r < 0.2 \Rightarrow \varepsilon < 0.01, V^{1/4} < 2.8 \times 10^{16} GeV$$

Standard inflation predicts Gaussian fluctuations

- The present inhomogeneities in the universe originate from quantum fluctuations of the inflaton field $\delta\phi\left(\vec{x},t\right)$:

$$\delta\phi\left(\vec{x},t\right)=\sum_{\vec{k}}\delta\phi_{\vec{k}}\left(t\right)e^{i\vec{k}\vec{x}}$$

Considering a generic perturbation $g\left(\vec{x},t\right)$ (e.g. the CMB temperature anisotropies ΔT) and its Fourier expansion

$$g\left(\vec{x},t\right)=\sum_{\vec{k}}g_{\vec{k}}\left(t\right)e^{i\vec{k}\vec{x}}$$

Using perturbation theory up to first order we can obtain $g_{\vec{k}}\left(t\right)$ in terms of the Fourier components of the inflaton field $\delta\phi_{\vec{k}}\left(t_{end}\right)$:

$$g_{\vec{k}}\left(t\right)=T\left(t,\vec{k}\right)\times\delta\phi_{\vec{k}}\left(t_{end}\right)$$

If each $\delta\phi_{\vec{k}}\left(t_{end}\right)$ is Gaussian and has no correlations among different modes $\vec{k}$ (as predicted by the standard slow-roll inflation) then any such generic perturbation will inherited those properties.

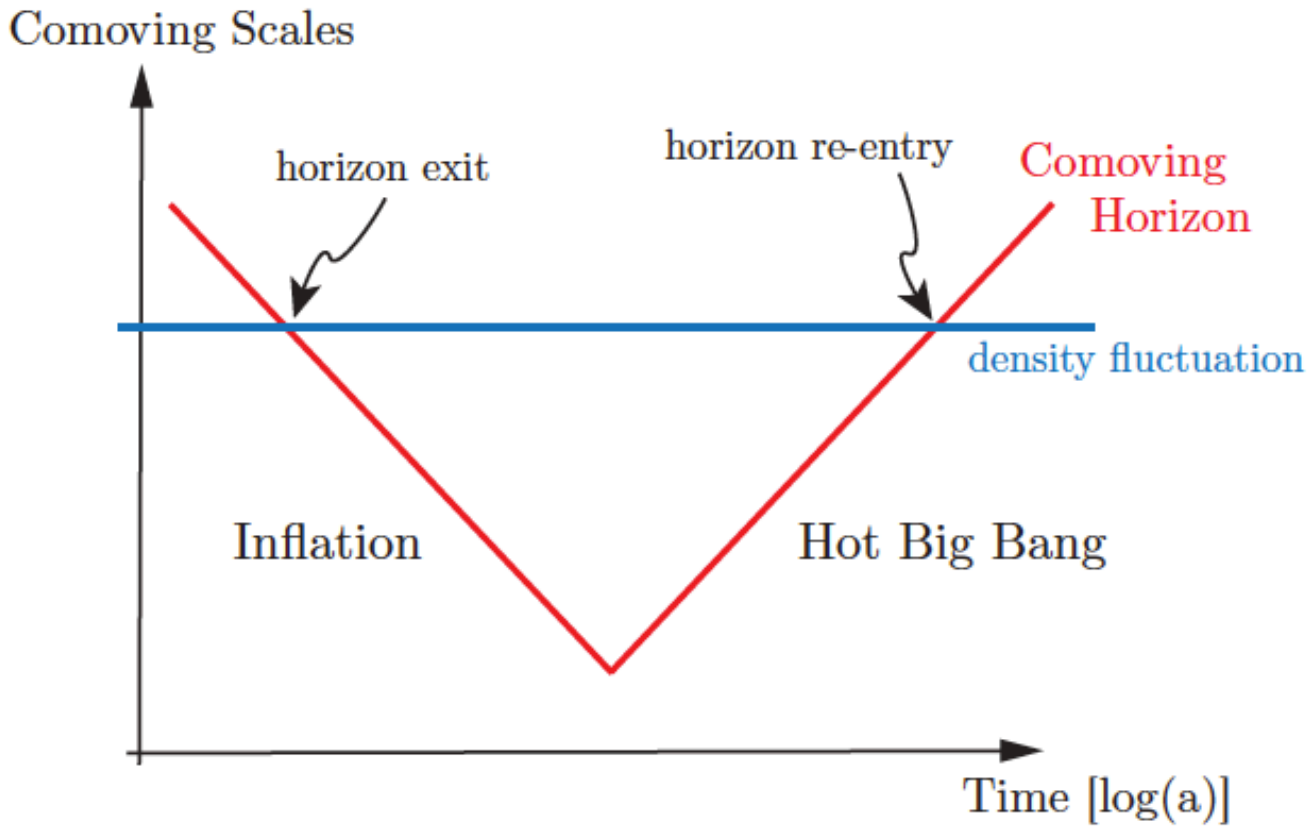

Creation and evolution of perturbations in the inflationary universe. Fluctuations are created quantum mechanically on sub-horizon scales. While comoving scales, k^{-1}, remain constant the comoving Hubble radius during inflation, $(aH)^{-1}$, shrinks and the perturbations exit the horizon. Causal physics cannot act on superhorizon perturbations and they freeze until horizon re-entry at late times.

Probing isotropy and Gaussianity

- Planck and the next generation of CMB polarization missions (e.g. COrE) will probe two important features of the current cosmological paradigm: the isotropy of the universe and the isotropy and Gaussianity of the primordial perturbations.
- There are two main approaches for testing the Isotropy and Gaussianity of the CMB:
  - Performing tests of the null hypothesis
  - Performing tests of alternative hypotheses
- There are many physical effects that might give rise to different deviations from isotropy and/or Gaussianity. The deviations might be classified according to their physical nature and origin as follows:
  - Non-standard inflationary models
  - Topological defects: cosmic strings, textures, …
  - Geometry and topology: Bianchi models, non-trivial topologies
  - Primordial magnetic fields

Tests of the null hypothesis

- There have been many tests of the null hypothesis (isotropy and Gaussianity) mainly based on the WMAP data. Although the two properties are very much tighten together, some tests try to focus on one property more than the other.
- Many analyses of the WMAP data using different statistical quantities have found deviations from the null hypothesis, what are generally known as WMAP anomalies. Some of the best studied ones are:
  - Low multipole alignment
  - Hemispherical asymmetry
  - The cold spot
  - Low variance
- Planck represents a unique opportunity to confirm or reject those anomalies (results are expected on January 2013).

Quadrupole and octopole planarity and alignment (“axis of evil”)

- The probability to find the quadrupole and octopole aligned with a separation angle < 10° is <1.5% (De Oliveira-Costa et al. 04, Schwartz 04, Slozar & Seljak 04, Land & Magueijo 05, 07, Copi et al. 06).
- Alignment direction (30°, 260°) and dipole direction (42°, 264°).
- It is not clear yet if the alignment is due to foregrounds, systematic effects or is of intrinsic origin.

Multipolar alignment

- De Oliveira-Costa et al. 04 assign directions to multipoles by maximizing the angular momentum dispersion:

$$\left\langle \left(L_z \Delta_l \right)^2 \right\rangle = \sum_m m^2 \left| a_{lm}\left(\vec{n}\right) \right|^2$$

$a_{lm}\left(\vec{n}\right)$ denotes the coefficients in a rotated system with the z axis in the direction $\vec{n}$. They find for the quadrupole and octopole directions separated by ≈10°.

Given a direction the probability of finding another one at random separated by an angle ≤10° es ≈1.5%! "Axis of evil"

Quadrupole

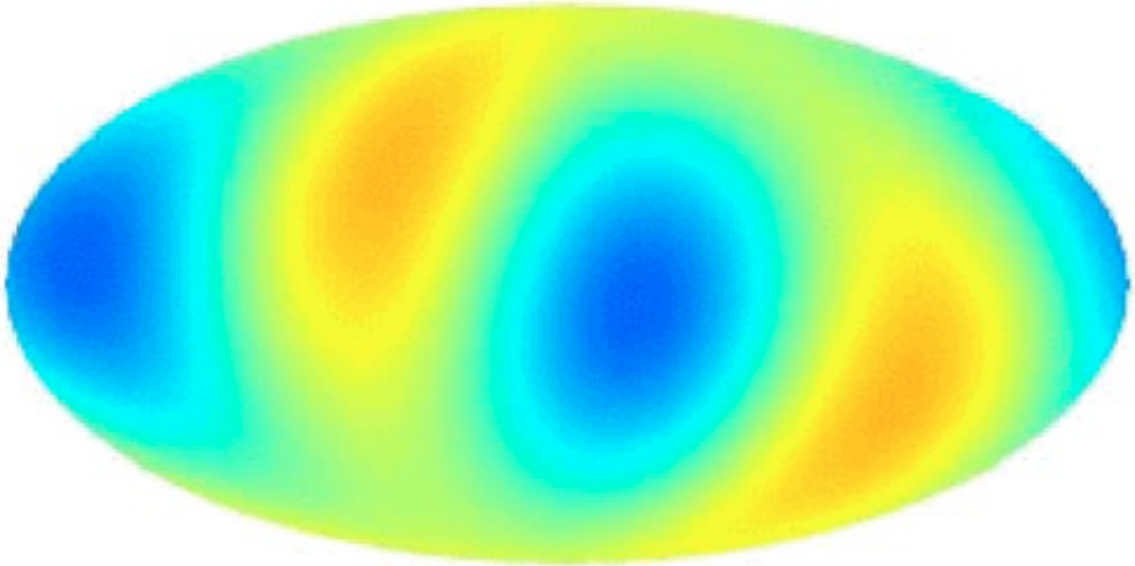

Octopole

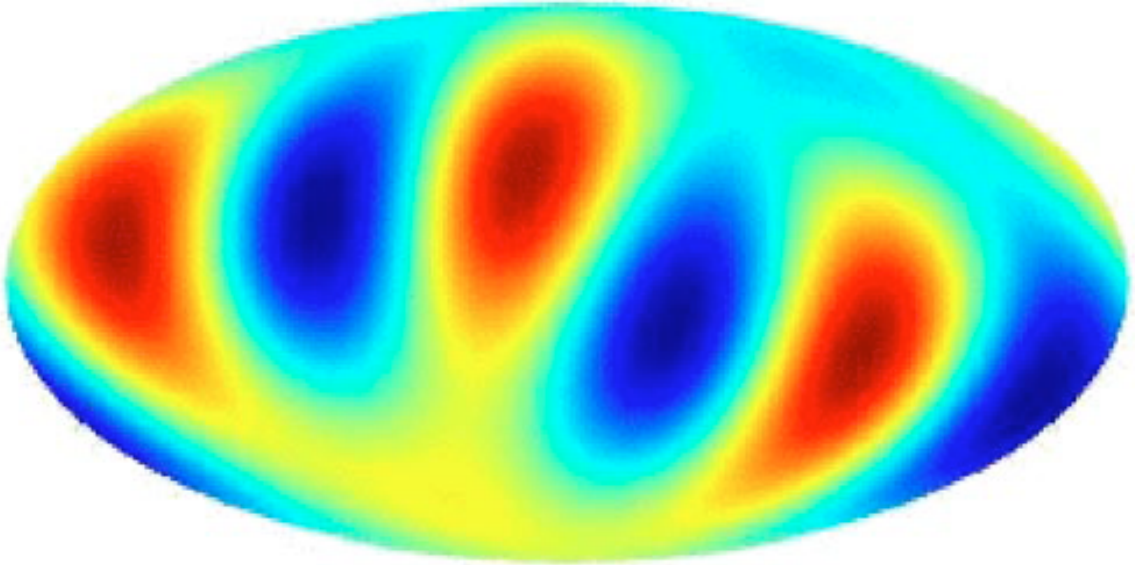

Hemispherical asymmetries in the local 2 and 3-point correlation functions and in the power spectrum

North-south assymmetries in ecliptic coordinates are found using:

- Local 2- and 3-point correlation functions (Eriksen et al. 2004a, 2005)
- Minkowski functionals (eriksen et al. 2004b)
- Local power spectrum (Hansen et al. 2004b, Donoghue and Donoghue 2005)
- Local curvature (Hansen et al. 2004a)

The asymmetry is maximum for a coordinate system with the North pole in the direction $(\theta, \varphi)=(80^o, 57^o)$, close to the ecliptic North pole $(60^o, 96^o)$.

North-south asymmetry

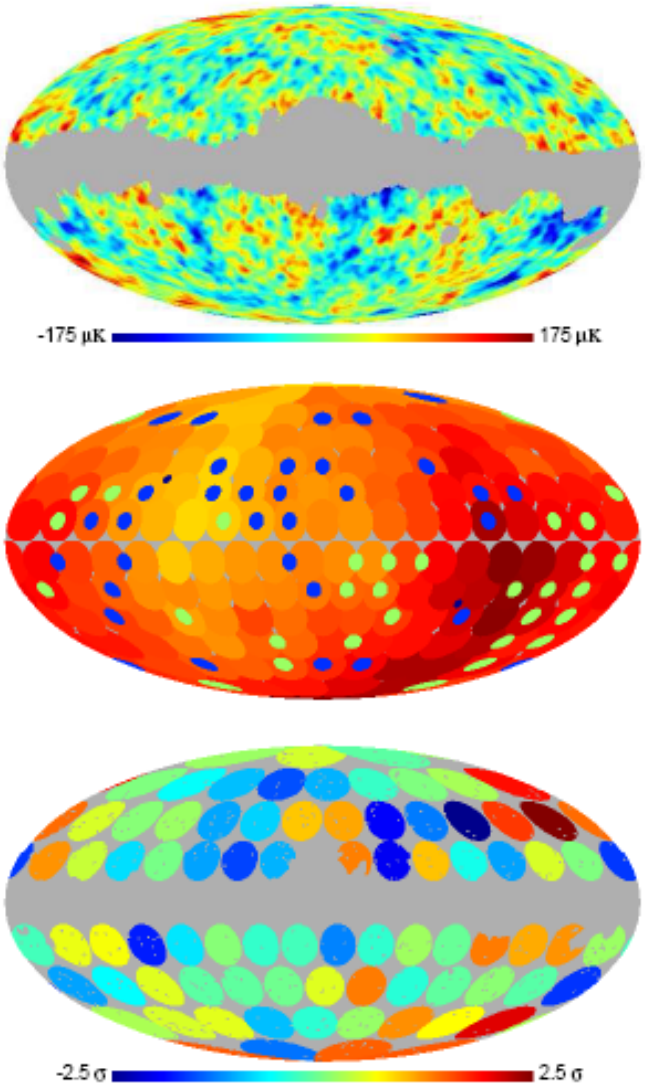

(Eriksen et al. 2004a)

Asymmetry axis

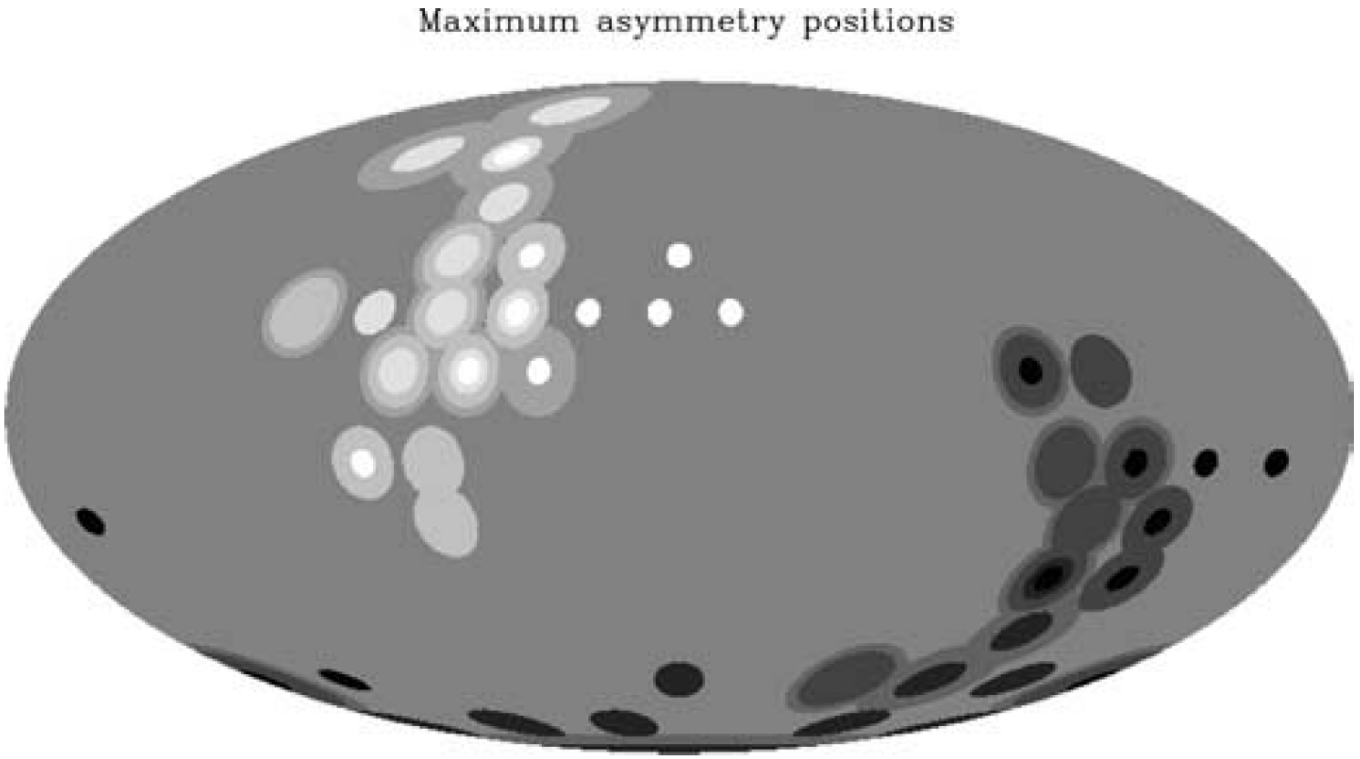

Hansen et al. 2004

Dipolar modulation

- Motivated by the hemispherical power asymmetry a dipole-modulated signal model has been tested (Hoftuft et al. 09):

$$\frac{\Delta T}{T}\left(\vec{n}\right) = \left[1 + A\left(\vec{n}.\vec{p}\right)\right]\frac{\Delta T}{T}^{iso}\left(\vec{n}\right) + n\left(\vec{n}\right)$$

After an intensive computation (working in real space), the best-fit modulation amplitud for $\ell \leq 64$ and the WMAP-5year ILC KQ85 sky cut is:

$$A = 0.072 \pm 0.022 \qquad (l,b) = (224^{\circ}, -22^{\circ}) \pm 24^{\circ}$$

See the poster by Raúl Fernández-Cobos about a possible dipolar modulation in the galaxy distribution traced by the NVSS radio galaxy catalogue.

Bianchi models

Jaffe et al. (2005, 2006)

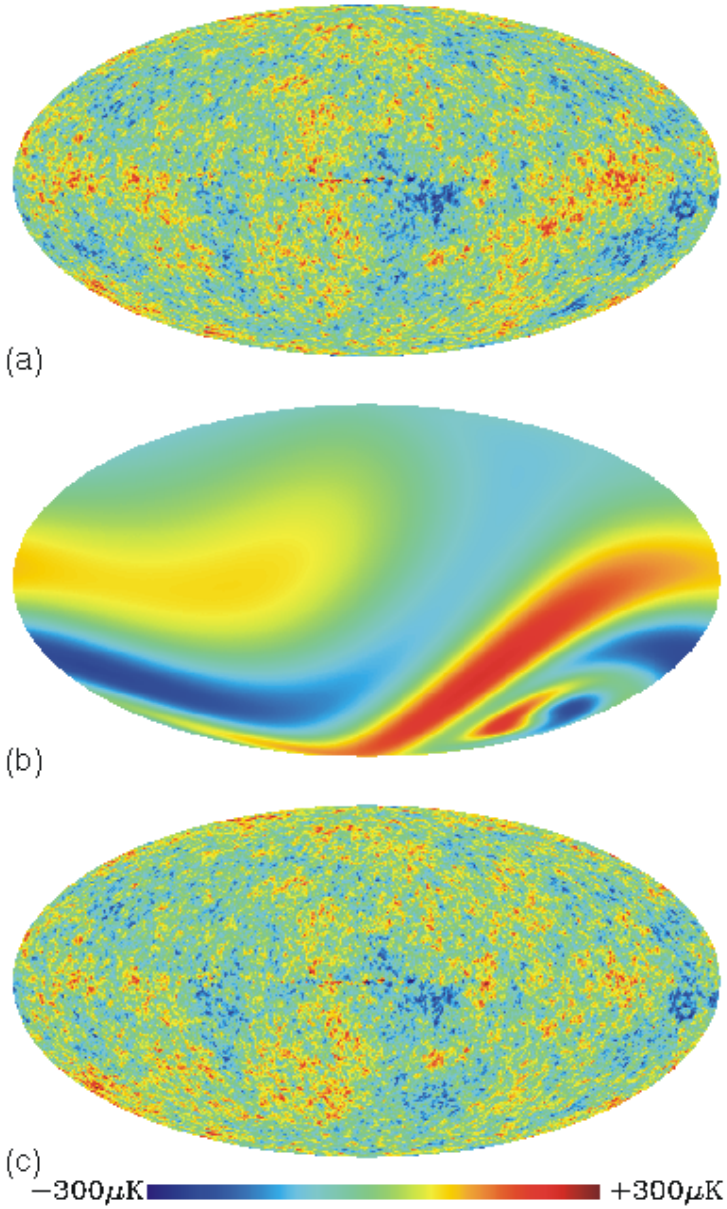

The universe is given by a perturbation of the FRW metric: it follows a Bianchi VII_h model, with a shear of 2.4E-10 and a right-hand vorticity of 4.3E-10, with a rotation axis in the direction (l,b)=(222º, -62º)

This models implies an Ω=0.5

Asymmetries

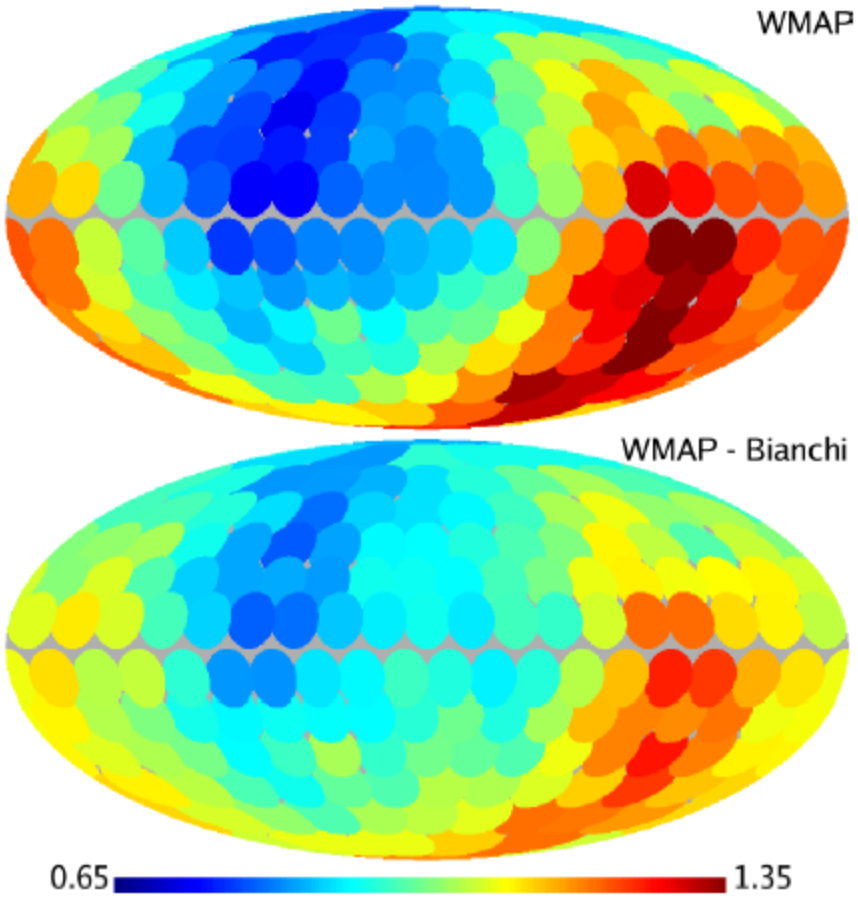

The cold spot

- **The first wavelet application to WMAP data was made by [Vielva et al. 2004]. Using the SMHW.**
- **A non-Gaussian detection was made on the kurtosis of the wavelet coefficients, at scales of around 5 degree**

Co-added WMAP

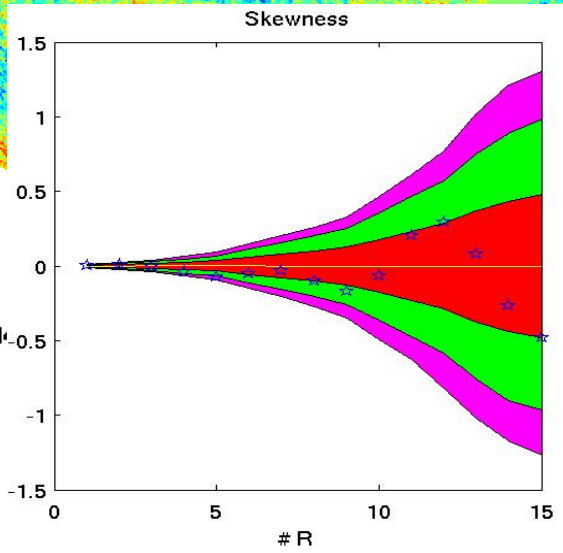

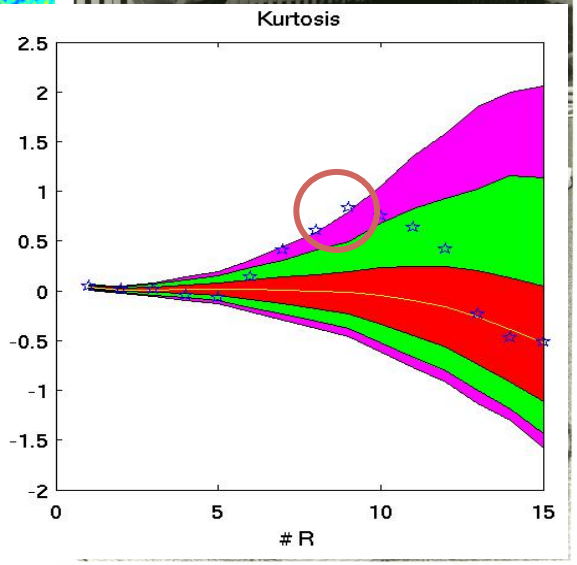

The cold spot

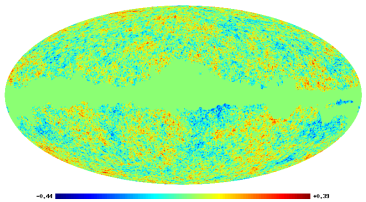

Co-added WMAP

- **It was showed that the detection was concentrated on the southern hemisphere, what can be understood as a breaking of isotropy,**
- **More recently, [Cruz et al. 2007] established that the probability of such detection is 1.85%, after analysing the 3-yr WMAP data**

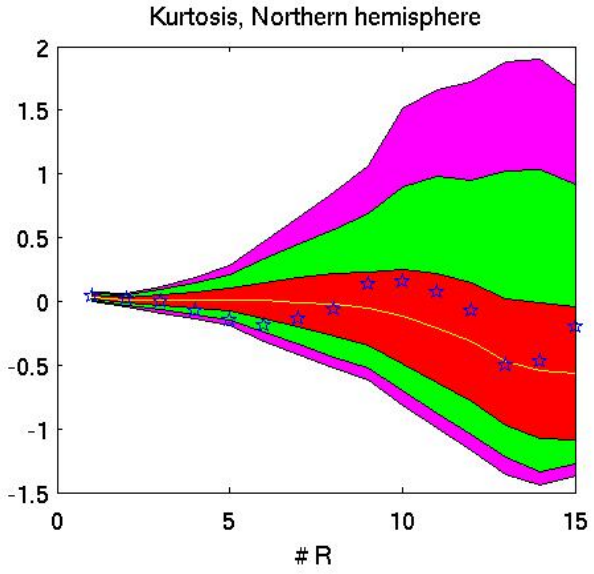

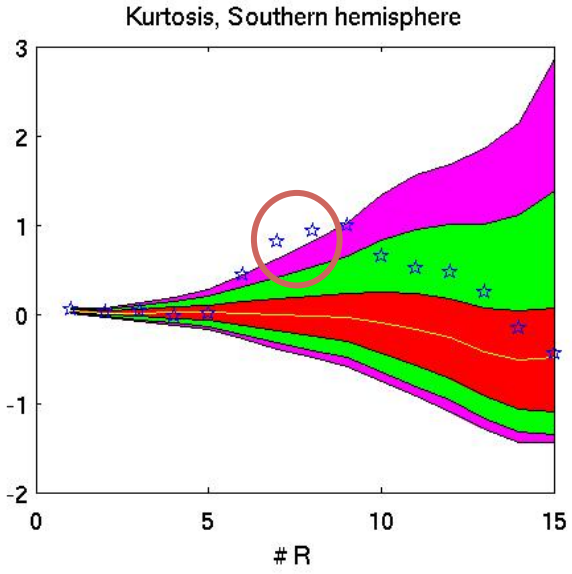

The cold spot

SMHW coefficients map @ R_8 = 250 arcmin above 3σ

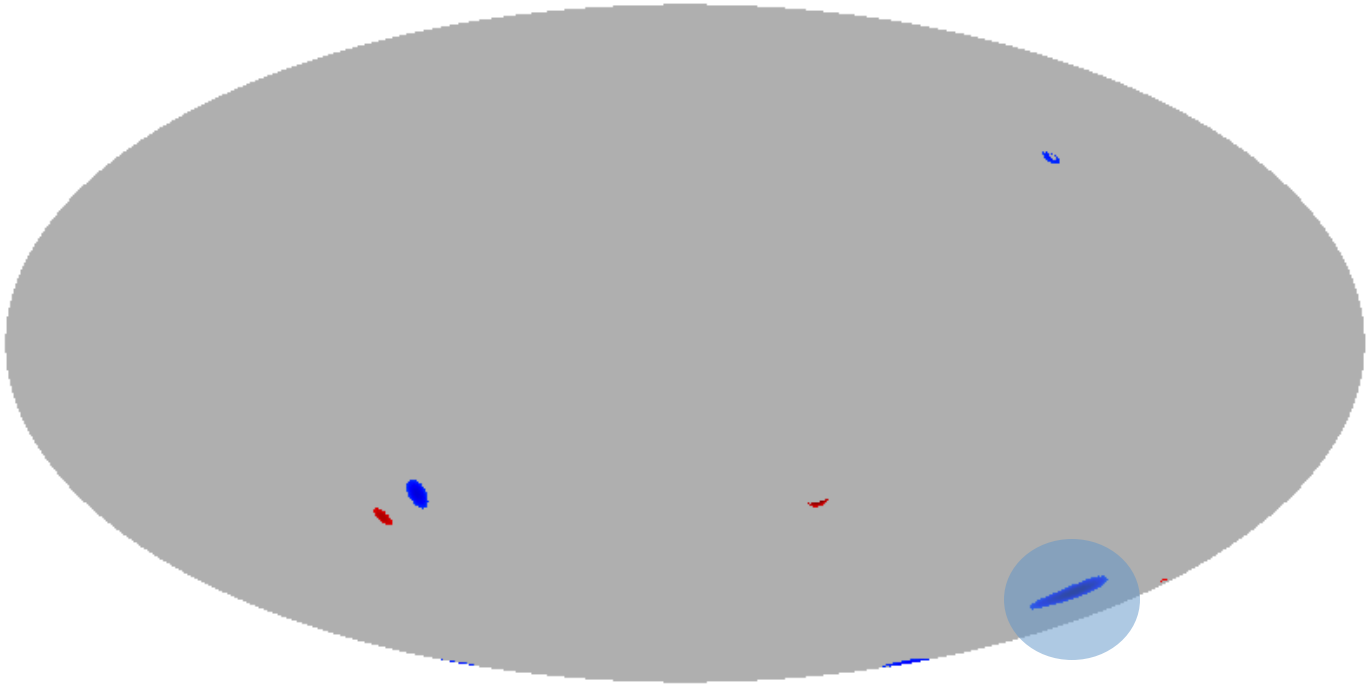

The Cold Spot

The effect of textures on the CMB

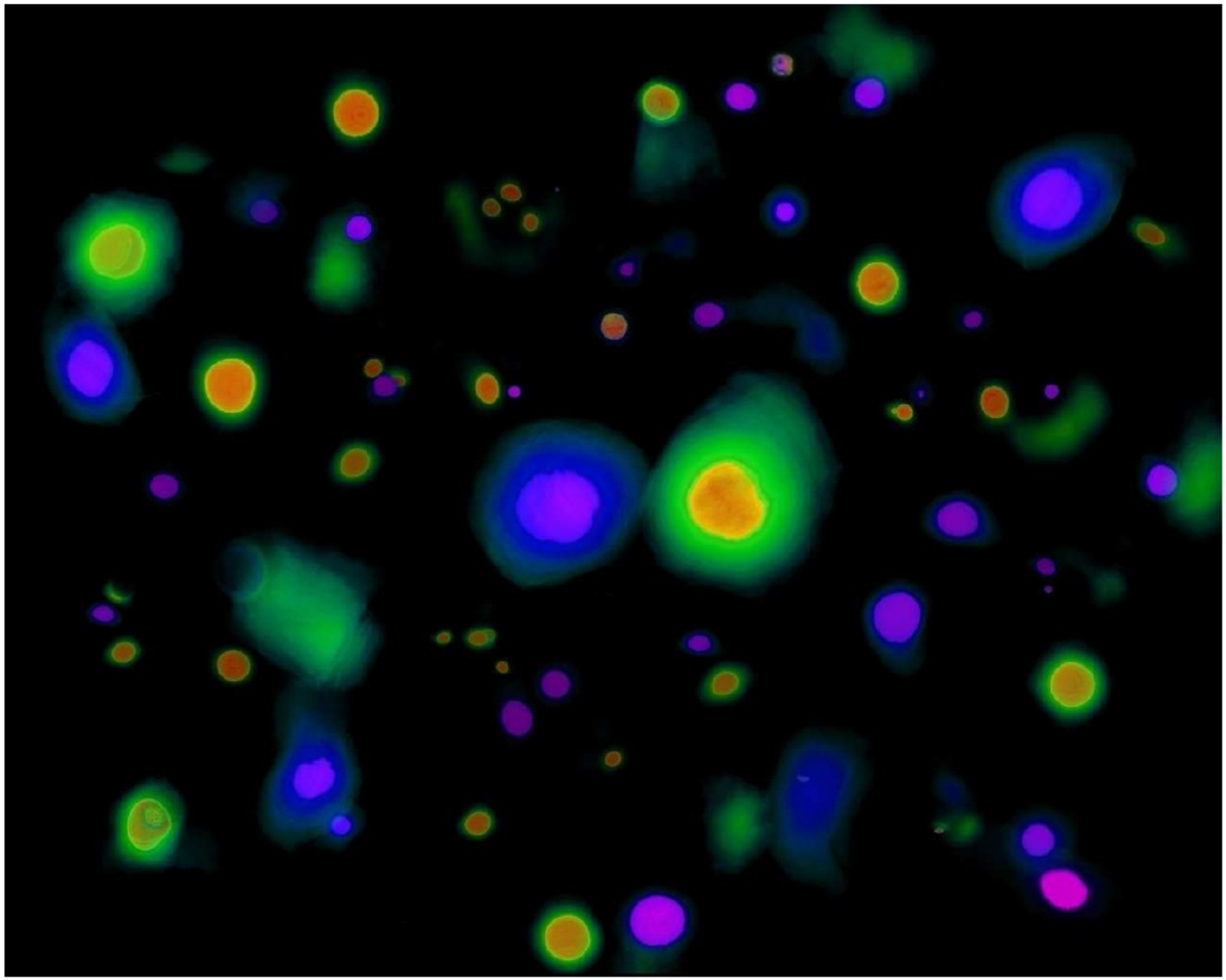

Is the cold spot caused by a texture?

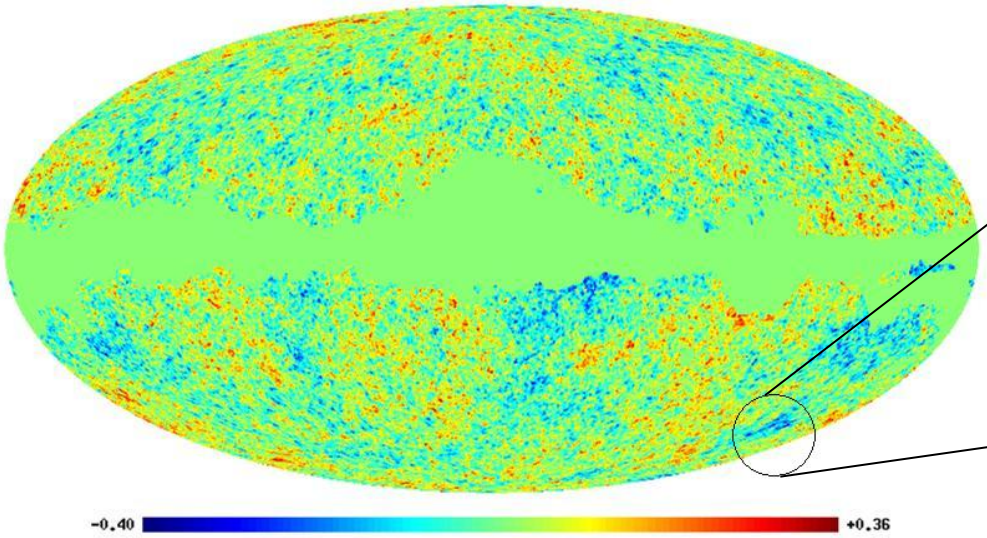

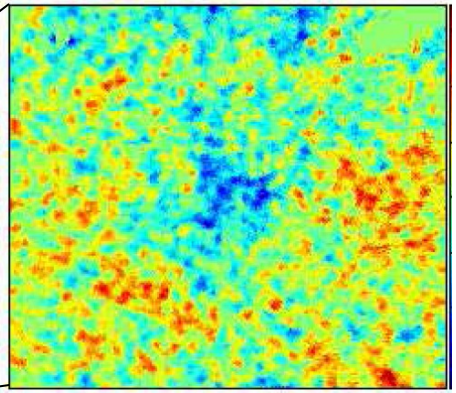

Texture template →

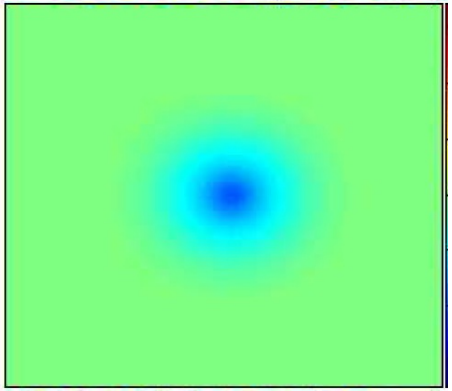

Data - Template →

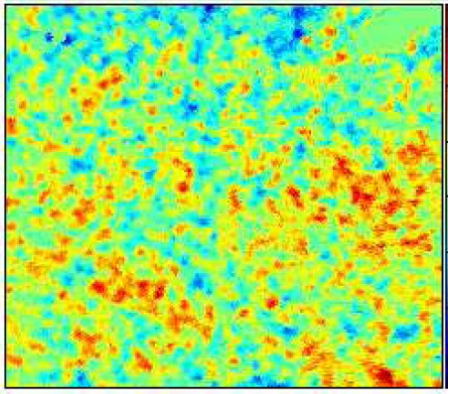

Martínez-González 2008, astro-ph/08054157

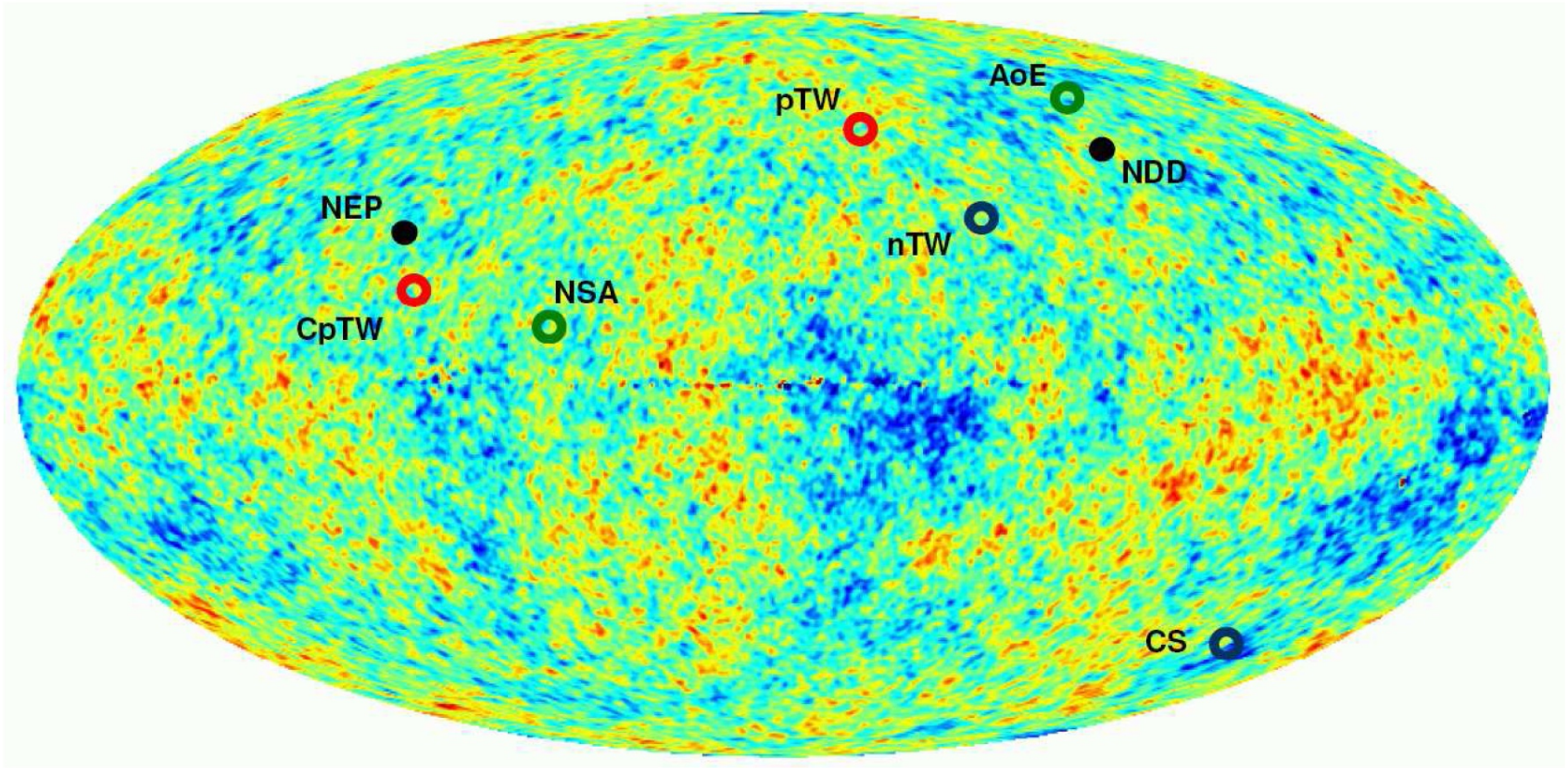

FIG. 4: Directions in the microwave sky derived from the anomalies found in WMAP data: northern direction of the North-South asymmetry (NSA), axis of evil (AoE), the cold spot (CS), cluster of positive total weights (CpTW), perpendicular axis to the positive total weights plane (pTW), perpendicular axis to the negative total weights plane (nTW). For reference the North ecliptic pole (NEP) and the northern direction of the CMB dipole (NDD) are also shown.

NON-STANDARD INFLATIONARY MODELS

- Assuming the FLRW metric and a homogeneous scalar field $\phi(t, \mathbf{x}) \equiv \phi(t)$ the energy-momentum takes the form of a perfect fluid:

$$\rho_\phi = \frac{1}{2}\dot{\phi}^2 + V(\phi)\,,$$
$$p_\phi = \frac{1}{2}\dot{\phi}^2 - V(\phi)\,.$$

- The simplest single-field slow-roll inflation can be extended in several ways:
  - Non-canonical kinetic terms
  - More than one field
  - Inhomogeneous reheating
  - Non-standard vacuum (excited state)

NON-STANDARD INFLATIONARY MODELS

- Multi-field scenarios (curvaton)
- Inhomogeneous reheating scenarios
- In these cases the GWB amplitude is expected to be undetectable and also $n_s \approx 1$ with high precision: it is not possible to extract information from the slow-roll parameters.
- There is a third observable: non-Gaussianity.

It is expected in the curvature perturbations at the second order:

$$\phi = \phi_L + f_{NL} \otimes \phi_L^2 + g_{NL} \otimes \phi_L^3$$

f_{NL} is the non-linear coupling parameter at first order and

g_{NL} is the one at second order.

Non-standard inflationary models (cont.)

- Large primordial non-Gaussianity can be generated if any of the conditions of canonical inflation is violated.
- The non-Gaussianity appears in higher-order moments like the bispectrum of the primordial perturbations of the gravitational potential *ϕ(k)*:

$$\left\langle \phi(k_1)\phi(k_2)\phi(k_3) \right\rangle = (2\pi)^3 \delta^3(k_1 + k_2 + k_3) f_{NL} F(k_1, k_2, k_3)$$

- Types of non-Gaussianity:
  - Local: $k_1 << k_2 \approx k_3$ e.g. multifield inflation, curvaton model, inhomogeneous reheating, hybrid inflation.
  - Equilateral: $k_1 \approx k_2 \approx k_3$ e.g. DBI inflation, ghost inflation.
  - Orthogonal: orthogonal to the local and equilateral cases.
- From WMAP 7-years data: (Komatsu et al. 2011)

$$f_{NL}^{local} = 32 \pm 21$$

$$f_{NL}^{equil} = 26 \pm 140$$

$$f_{NL}^{orthog} = -202 \pm 104$$

- Consistent results obtained with other techniques (e.g. wavelets, neural networks): Curto et al. 2011, Casaponsa et al. 2011
- A f_{NL} detection of the local type would rule our all single-field inflation models! (Creminelli & Zaldarriaga 2004)

Shape functions: local, equilateral, orthogonal

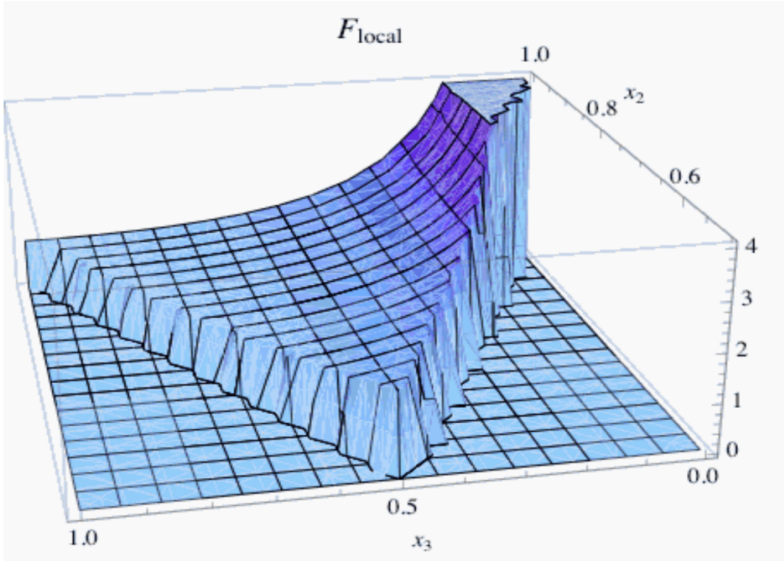

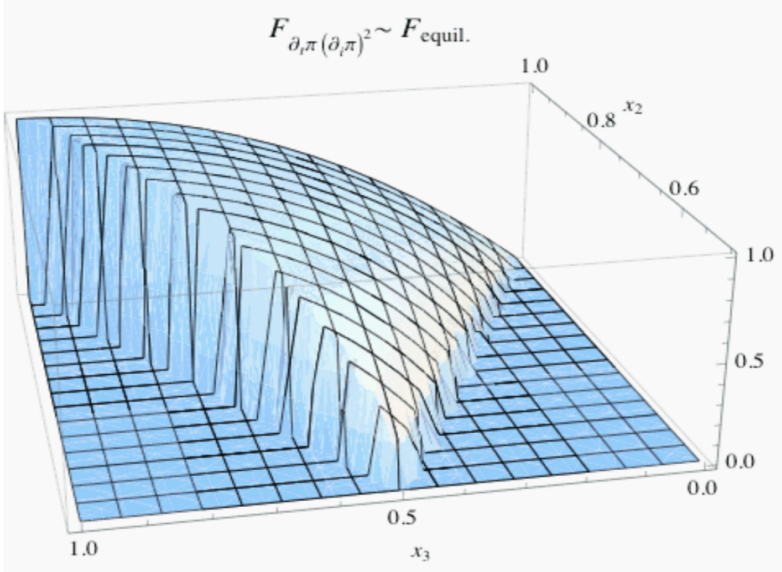

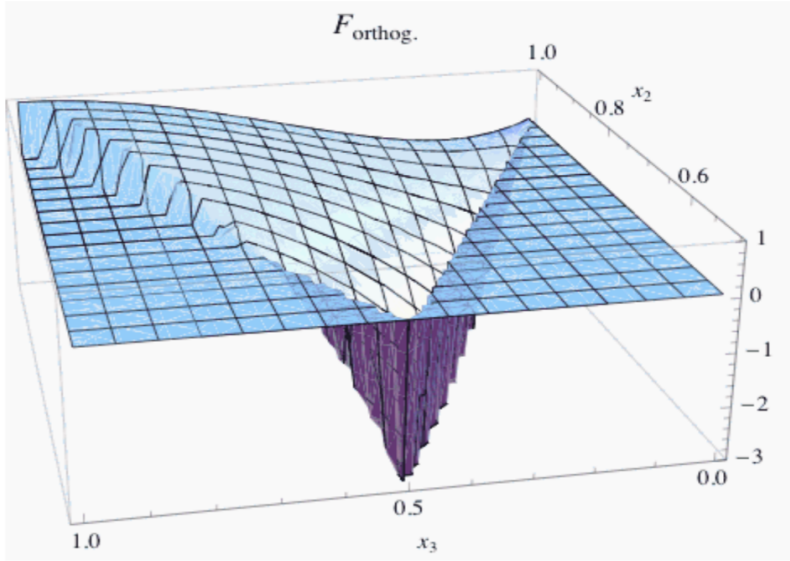

$$f_{NL}=0$$

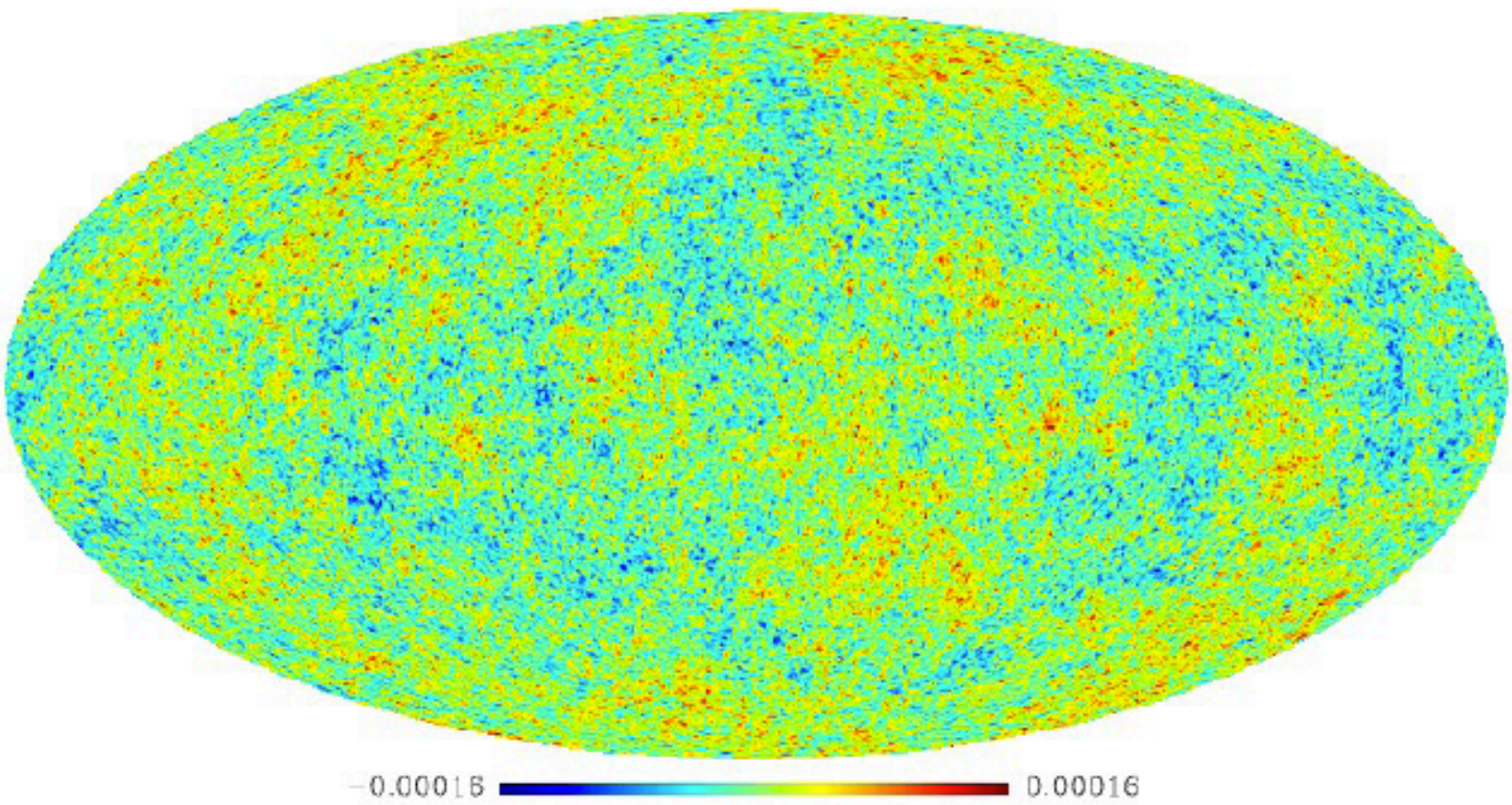

Liguori, Yadav, Hansen, Komatsu, Matarrese, Wandelt, PRD (2007)

$$f_{NL}=10^{1}$$

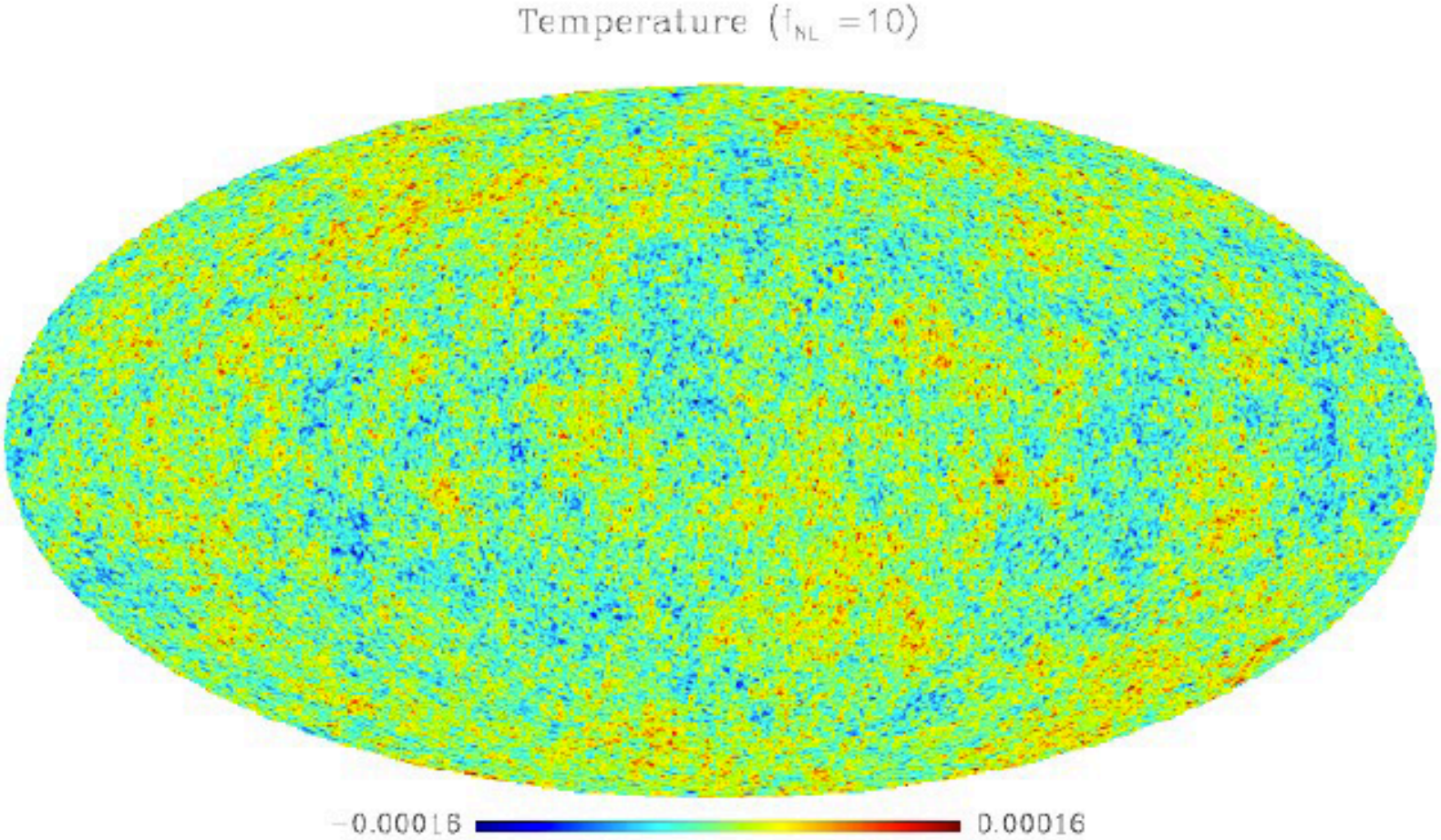

Liguori, Yadav, Hansen, Komatsu, Matarrese, Wandelt, PRD (2007)

$$f_{NL}=10^2$$

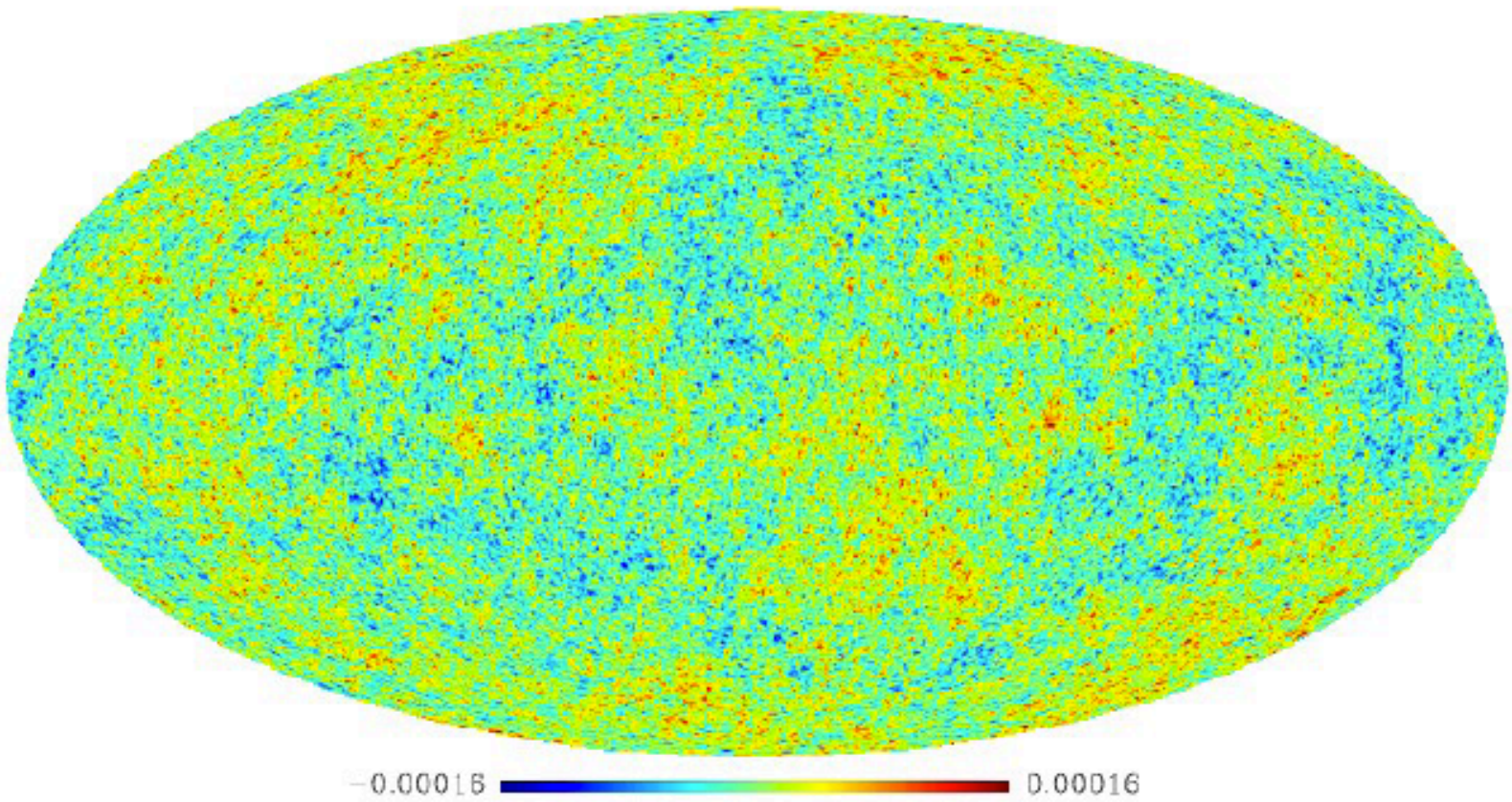

Liguori, Yadav, Hansen, Komatsu, Matarrese, Wandelt, PRD (2007)

$$f_{NL} = 10^3$$

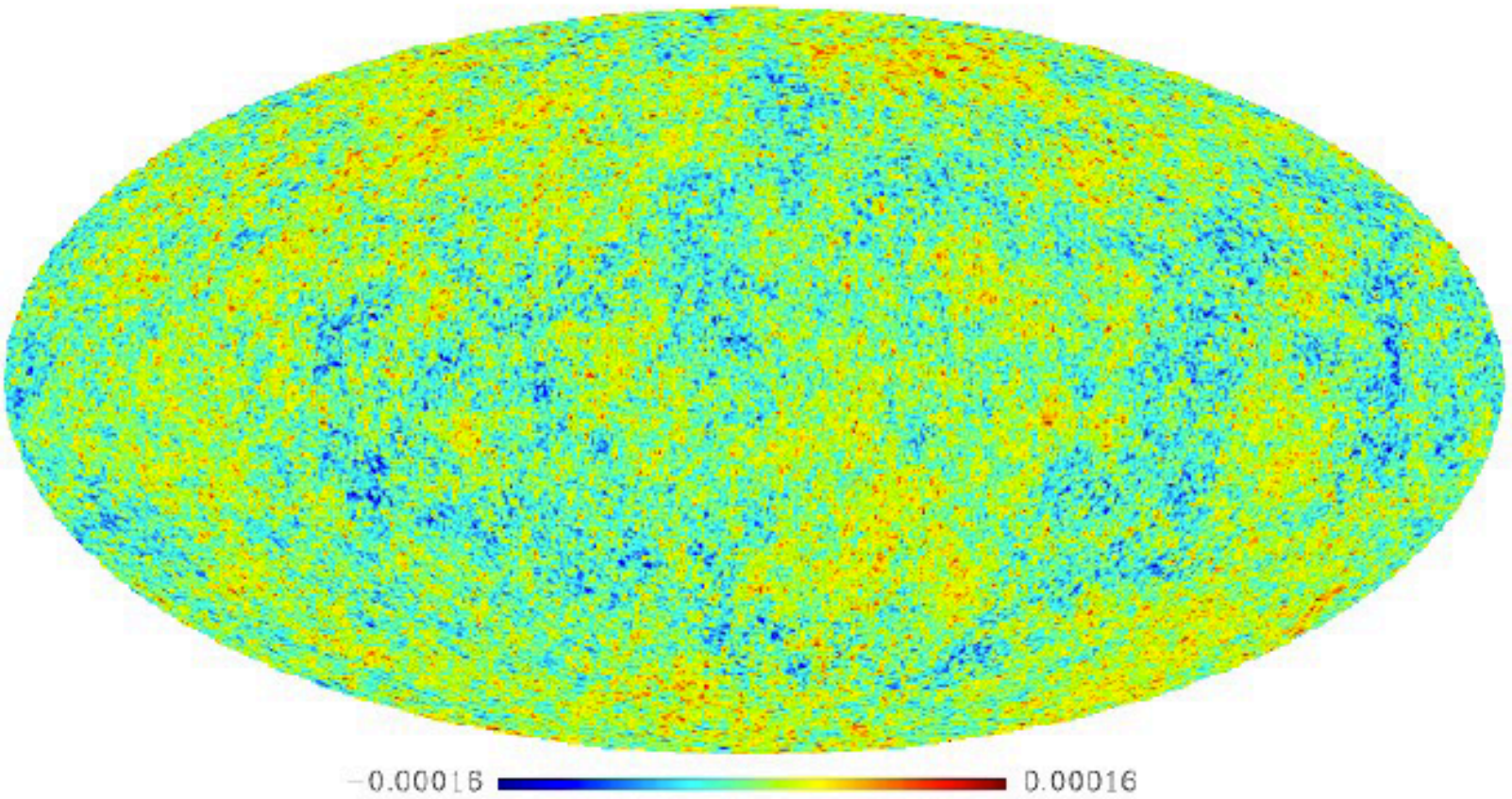

Liguori, Yadav, Hansen, Komatsu, Matarrese, Wandelt, PRD (2007)

Transfer function

- The primordial gravitational potential Φ is related to the CMB multipoles $a_{\ell m}$ by a convolution with the transfer function $g_\ell(k)$ (see e.g. Yadav & Wandelt 10)

$$a_{\ell m} = 4\pi(-1)^\ell \int \frac{d^3k}{(2\pi)^3} \Phi\left(\vec{k}\right) g_\ell(k) Y^*_{\ell m}\left(\hat{k}\right)$$

The radiation transfer function $g_\ell(k)$ includes all the linear order effects, like the Sachs-Wolfe effect, Integrated Sachs-Wolfe effect, acoustic peaks and Silk damping. Similarly, an equivalent relation can be found for the E-mode polarization CMB multipoles by replacing the temperature tranfer function by the polarization one.

The bispectrum

- The bispectrum represents the lowest-order correlator to probe non-Gaussianity. Most models of inflation make specific predictions for it. It is defined by:

$$B^{\ell_1\ell_2\ell_3}_{m_1m_2m_3} = \left\langle a_{\ell_1 m_1} a_{\ell_2 m_2} a_{\ell_3 m_3} \right\rangle$$

- Most theories assume isotropy and therefore the angular average bispectrum is usually considered:

$$B_{\ell_1\ell_2\ell_3} = \sum_{m_1m_2m_3} \begin{pmatrix} \ell_1 \ell_2 \ell_3 \\ m_1 m_2 m_3 \end{pmatrix} \left\langle a_{\ell_1 m_1} a_{\ell_2 m_2} a_{\ell_3 m_3} \right\rangle$$

- Another convenient quantity is the reduced bispectrum:

$$B^{\ell_1\ell_2\ell_3}_{m_1m_2m_3} = G^{\ell_1\ell_2\ell_3}_{m_1m_2m_3} b_{\ell_1\ell_2\ell_3}$$

where $G^{\ell_1\ell_2\ell_3}_{m_1m_2m_3}$ is the Gaunt integral.

- The bispectrum including polarization can be defined in a similar way. Possible components are: TTT, TTE, TEE, EEE.

f_{NL} estimation

- In the limit of weak non-Gaussianity the optimal bispectrum estimator for f_{nl} can be obtained by performing an Edgeworth expansion of the pdf (Babich 2005):

$$P(a \mid f_{nl}) = \left[1 - f_{nl} \sum_{\ell_i m_i} \left\langle a_{\ell_1 m_1} a_{\ell_2 m_2} a_{\ell_3 m_3} \right\rangle_{f_{nl}=1} \frac{\partial}{\partial a_{\ell_1 m_1}} \frac{\partial}{\partial a_{\ell_2 m_2}} \frac{\partial}{\partial a_{\ell_3 m_3}} + O\left(f_{nl}^2\right)\right] \frac{\exp\left(-\frac{1}{2} \sum_{\ell_i m_i} a^*_{\ell_4 m_4} C^{-1}_{\ell_4 m_4, \ell_5 m_5} a_{\ell_5 m_5}\right)}{(2\pi)^{N/2} \det(C)^{1/2}}$$

$C = C^{CMB} + C^{noise}$ is the signal plus noise power spectrum.

- A necessary and sufficient condition to saturate the Cramer-Rao inequality is given by the condition:

$$\frac{\partial \log P(a \mid f_{nl})}{\partial f_{nl}} = F_{f_{nl} f_{nl}}(a)\left(\hat{f}_{nl} - f_{nl}\right)$$

where *F* is the fisher matrix:

$$F_{f_{nl} f_{nl}}(a) = \left\langle \frac{\partial^2 \ln p(a \mid f_{nl})}{\partial f_{nl}^2} \right\rangle$$

f_{NL} optimal estimation

- The optimal f_{NL} estimator has been shown to be (Babich 2005, Creminelli et al. 2006):

$$\hat{f}_{NL} = \frac{1}{N} \sum_{\ell_i m_i} \left[\left\langle a_{\ell_1 m_1} a_{\ell_2 m_2} a_{\ell_3 m_3} \right\rangle_{f_{nl}=1} \left(C^{-1}_{\ell_1 m_1, \ell_4 m_4} C^{-1}_{\ell_2 m_2, \ell_5 m_5} C^{-1}_{\ell_3 m_3, \ell_6 m_6} a_{\ell_4 m_4} a_{\ell_5 m_5} a_{\ell_6 m_6} - 3 C^{-1}_{\ell_1 m_1, \ell_2 m_2} C^{-1}_{\ell_3 m_3, \ell_4 m_4} a_{\ell_4 m_4} \right) \right]$$

  However, for some real situations involving millions of data and complex masks and noise the optimal estimator may be unfeasible to compute and other reduced estimators can be more convenient (e.g. KSW, wavelet, modal, binned).

- The KSW (Komatsu, Spergel and Wandelt 2005) assumes a diagonal covariance matrix and when generalized with a linear term takes the form (Creminelli et al. 2006):

$$\hat{f}_{NL} = \frac{1}{N} \sum_{\ell_i m_i} \left[\left\langle a_{\ell_1 m_1} a_{\ell_2 m_2} a_{\ell_3 m_3} \right\rangle_{f_{nl}=1} \left(C^{-1}_{\ell_1} C^{-1}_{\ell_2} C^{-1}_{\ell_3} a_{\ell_1 m_1} a_{\ell_2 m_2} a_{\ell_3 m_3} - 3 C^{-1}_{\ell_1} C^{-1}_{\ell_2} C^{-1}_{\ell_3} C_{\ell_1 m_1, \ell_2 m_2} a_{\ell_3 m_3} \right) \right]$$

The wavelet estimator

- Wavelets are very useful analysing tools for their spatial-scale localization.
- The Spherical Mexican Hat Wavelets (SMHW), defined in the plane by the second derivative of the Gaussian and projected to the sphere by a stereographic projection, are very compact in both real and harmonic spaces.
- They also show a good decorretation of their coefficients at distances above the scale of the wavelet.
- From the wavelet coefficients $w(\vec{b}, R_i)$ (mean subtracted) we can construct the third order statistics:

$$q_{ijk} = \frac{1}{\sigma_i \sigma_j \sigma_k} \int w(\vec{b}, R_i) w(\vec{b}, R_j) w(\vec{b}, R_k) d\vec{b}$$

and combine them in a χ^2 test:

$$\chi^2(f_{nl}) = \sum_{ijk,rst} (q_{ijk} - \langle q_{ijk} \rangle_{f_{nl}}) C^{-1}_{ijk,rst} (q_{rst} - \langle q_{rst} \rangle_{f_{nl}})$$

The estimator is

$$\hat{f}_{NL} = \frac{\sum_{ijk,rst} \langle q_{ijk} \rangle_{f_{NL}=1} C^{-1}_{ijk,rst} q_{rst}}{\sum_{ijk,rst} \langle q_{ijk} \rangle_{f_{NL}=1} C^{-1}_{ijk,rst} \langle q_{rst} \rangle_{f_{NL}=1}}$$

SMHW properties

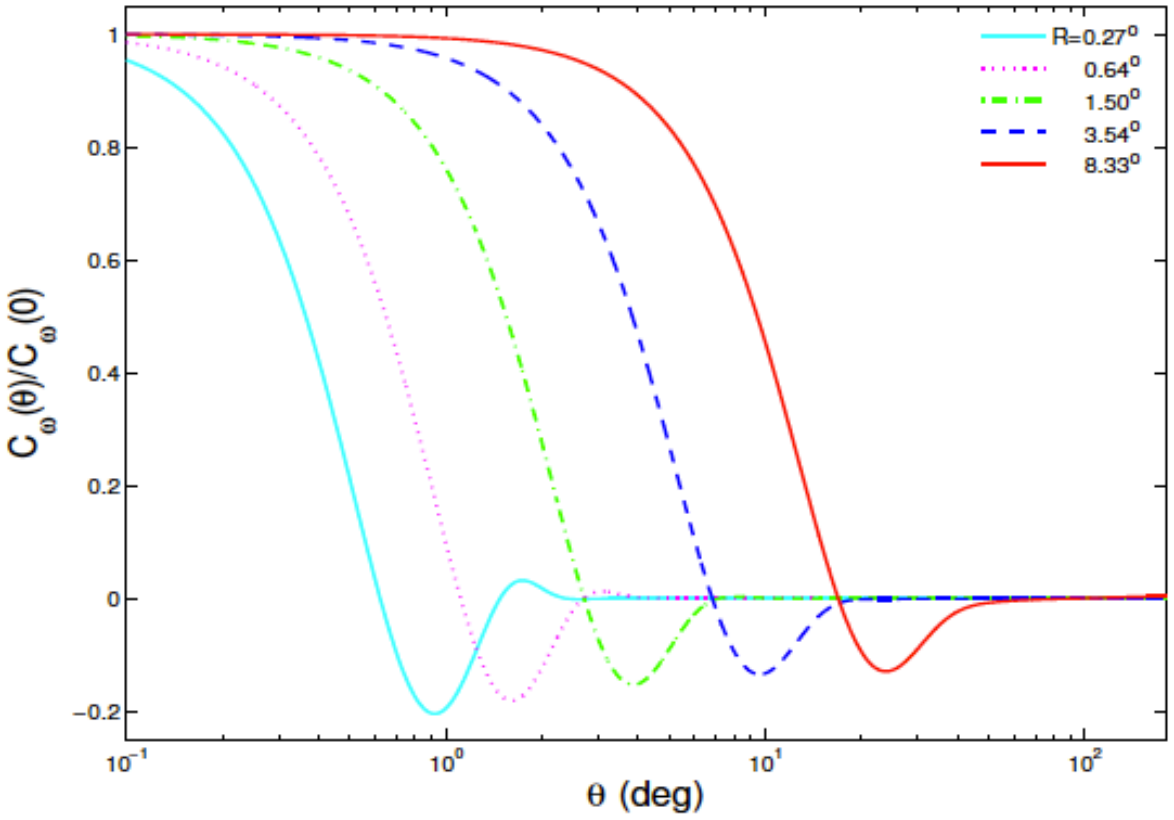

SMHW properties

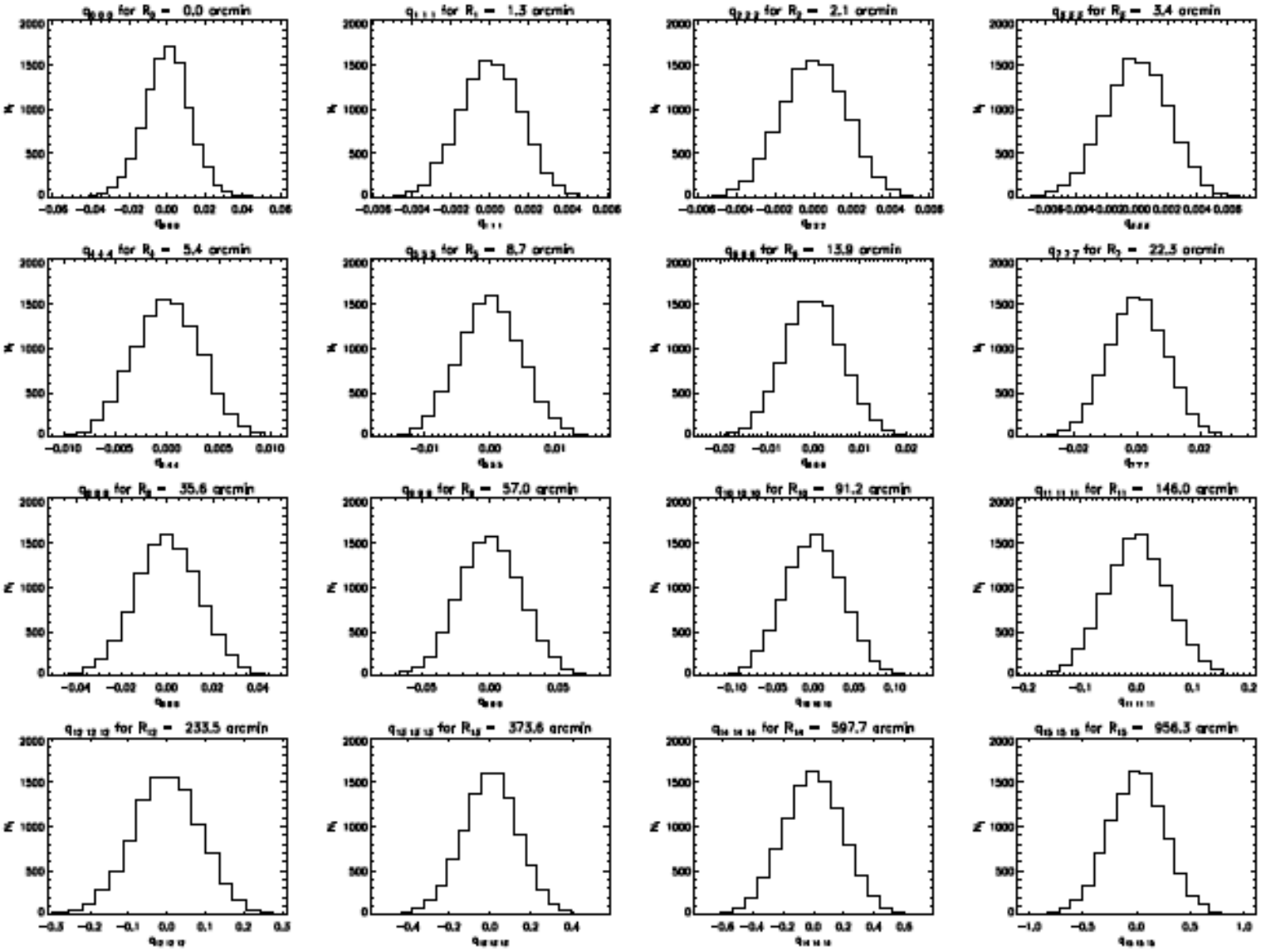

Linear term

- The variance of a cubic estimator can be improved if a linear term is included (Wick´s product).
- A linear term naturally appears in the derivation of the optimal estimator

$$\hat{f}_{NL}=\frac{1}{N}\sum_{\ell_i m_i}\left\{B_{l_1 l_2 l_3}^{f_{NL}=1}\begin{pmatrix} l_1 & l_2 & l_3 \\ m_1 & m_2 & m_3 \end{pmatrix}\left[\left(C^{-1}a\right)_{l_1 m_1}\left(C^{-1}a\right)_{l_2 m_2}\left(C^{-1}a\right)_{l_3 m 3}-3C^{-1}_{l_1 m_1, l_2 m_2}\left(C^{-1}a\right)_{l_3 m_3}\right]\right\}$$

  and it is incorporated when a diagonal covariance is assumed (Creminelli et al. 2006)

$$\hat{f}_{NL}=\frac{1}{N}\sum_{\ell_i m_i}\left[\left\langle a_{\ell_1 m_1}a_{\ell_2 m_2}a_{\ell_3 m_3}\right\rangle_{f_{nl}=1}\left(C^{-1}_{\ell_1}C^{-1}_{\ell_2}C^{-1}_{\ell_3}a_{\ell_1 m_1}a_{\ell_2 m_2}a_{\ell_3 m_3}-3C^{-1}_{\ell_1}C^{-1}_{\ell_2}C^{-1}_{\ell_3}C_{\ell_1 m_1,\ell_2 m_2}a_{\ell_3 m_3}\right)\right]$$

- For all-sky and isotropic noise the linear term is the monopole and thus zero.
- For maks and noise anisotropies similar to those of WMAP or Planck the linear term is of the order of the cubic term.
- For the SMHW a linear term can be also incorporated and it is equivalent to subtract the mean value of the wavelet coefficients at each scale (Curto et al. 2011). However for needlets the contribution is not negligible (Donzelli et al. 2012).

WMAP KQ75 mask and V+W anisotropic noise

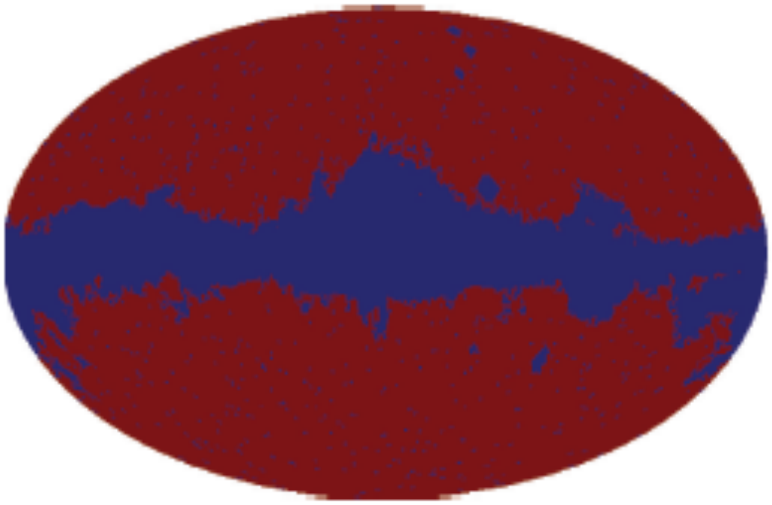

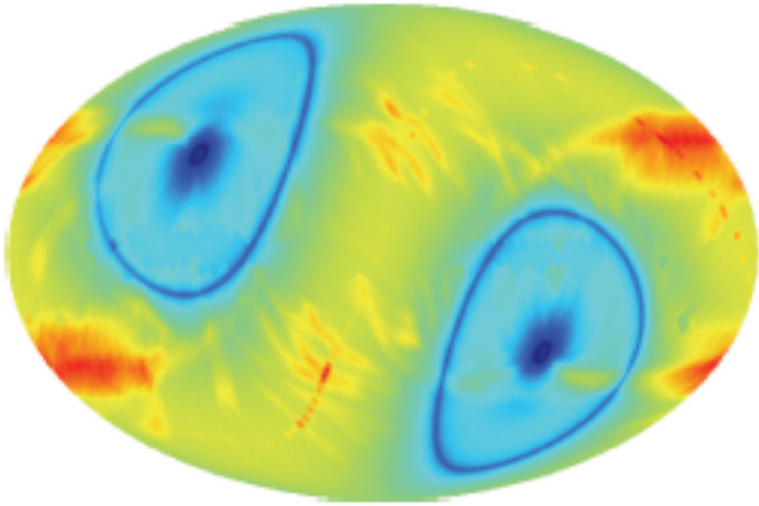

f_{NL} estimation with wavelets

- The wavelet estimator has been proved to be optimal (within a few percent) and has provided results consistent with the optimal harmonic estimator for WMAP (Curto et al. 2011).

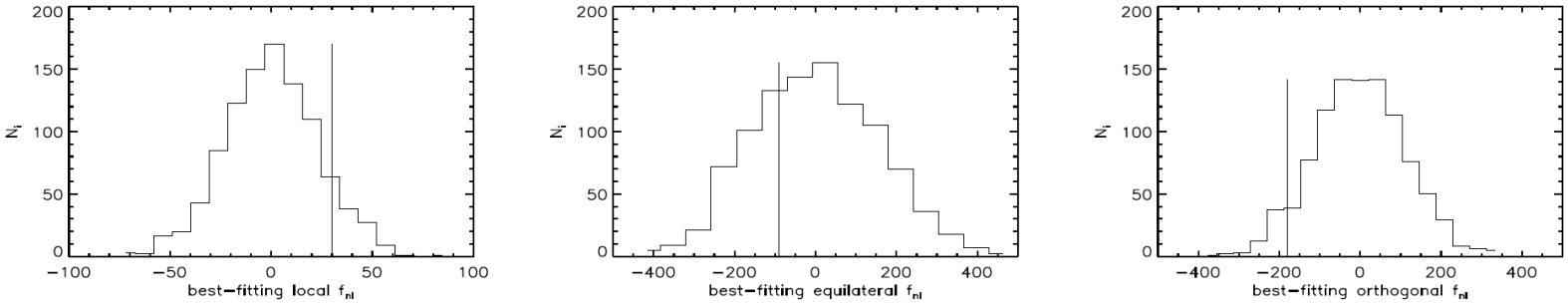

- The estimate of the contribution of point sources have been studied with this technique using the de Zotti et al. model for radio galaxies:

$$\Delta f_{NL}^{local} = 2.5 \pm 3 \Rightarrow f_{NL}^{local} = 30 \pm 22$$

$$\Delta f_{NL}^{equil} = 37 \pm 18 \Rightarrow f_{NL}^{equil} = -90 \pm 146$$

$$\Delta f_{NL}^{orthog} = 25 \pm 14 \Rightarrow f_{NL}^{orthog} = -180 \pm 107$$

Planck sensitivity to f_{NL}

(1-year of data)

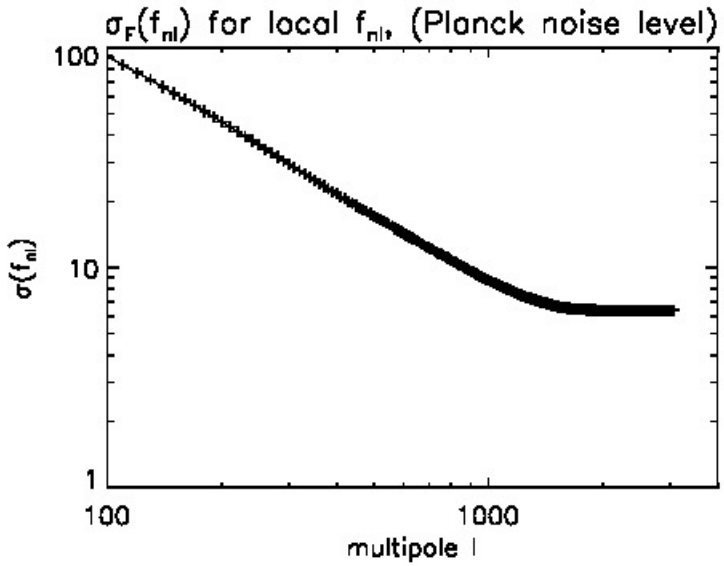

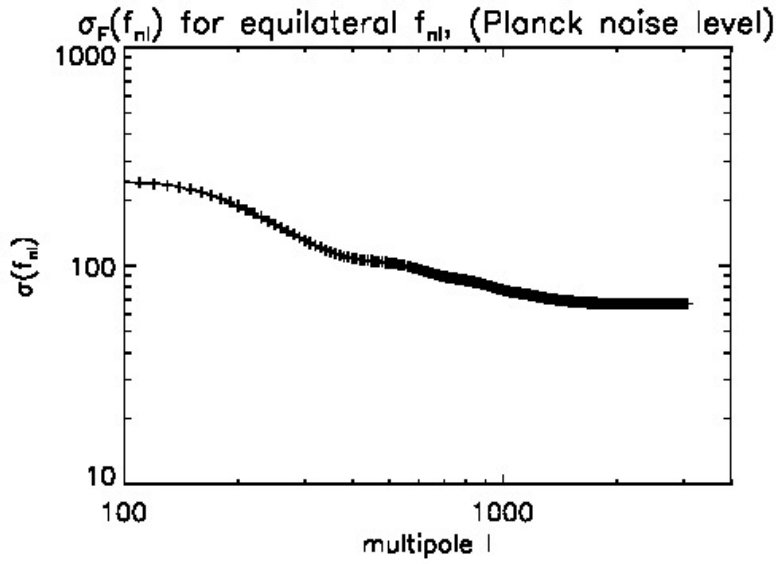

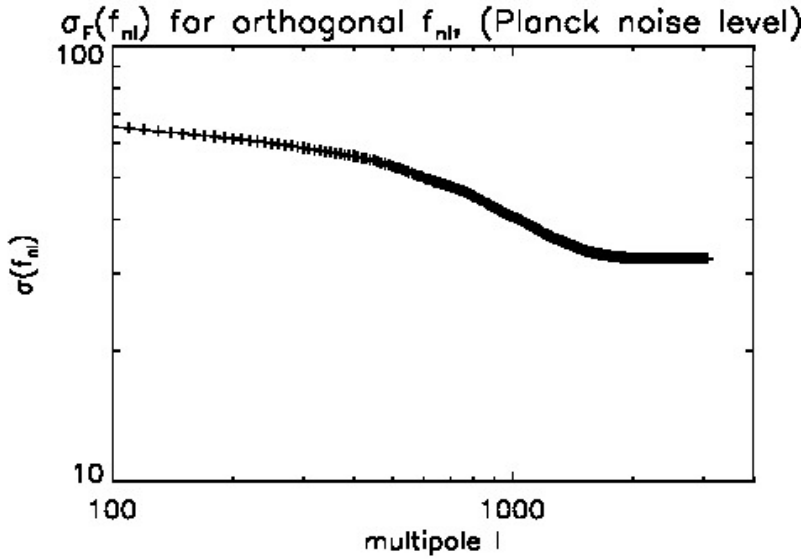

(Curto, M-G, Barreiro 2011)

Including polarization

- The general bispectrum for temperature *T* and polarization *E* is defined as:

$$B^{pqr}_{\ell_1\ell_2\ell_3,m_1m_2m_3} = \left\langle a^p_{\ell_1 m_1} a^q_{\ell_2 m_2} a^r_{\ell_3 m_3} \right\rangle$$

where *p,q,r=T,E*. Similarly for the angular-averaged bispectrum.

$$B^{pqr}_{\ell_1\ell_2\ell_3} = \sum_{m_1m_2m_3} \begin{pmatrix} \ell_1\ell_2\ell_3 \\ m_1m_2m_3 \end{pmatrix} \left\langle a^p_{\ell_1 m_1} a^q_{\ell_2 m_2} a^r_{\ell_3 m_3} \right\rangle$$

- The same procedure that was followed to derive the bispectrum estimator for only *T* applies also to (*T,E*). In particular optimal errors can be estimated by the Fisher matrix:

$$\frac{1}{\sigma^2} = \sum_{ijk,pqr} \sum_{\ell_1 \le \ell_2 \le \ell_3} \frac{1}{\Delta_{\ell_1\ell_2\ell_3}} B^{ijk}_{\ell_1\ell_2\ell_3} \left(Cov^{-1}\right)_{ijk,pqr} B^{pqr}_{\ell_1\ell_2\ell_3}$$

where $\Delta_{\ell_1\ell_2\ell_3} = 1 + 2\delta_{\ell_1\ell_2}\delta_{\ell_2\ell_3} + \delta_{\ell_1\ell_2} + \delta_{\ell_2\ell_3} + \delta_{\ell_1\ell_3}$

f_{NL} sensitivity witn *T,E*

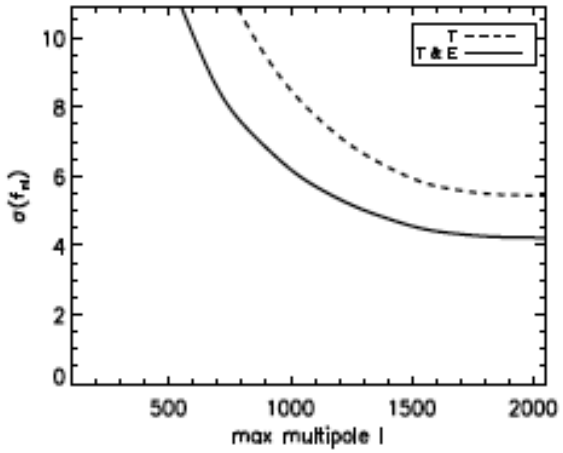

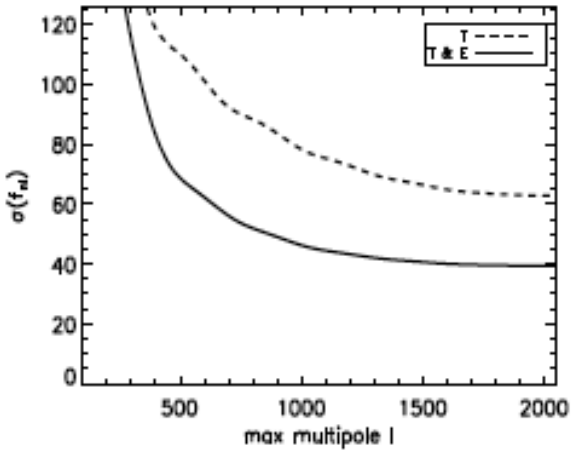

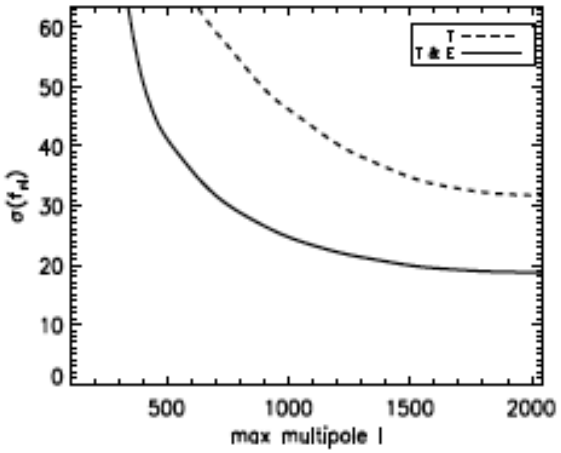

These sensitivites are for Planck 143 GHz. The values should be also divided by $f_{sky}^{1/2}$.

(Curto & EMG 2011)

Secondary effects

- The ISW-lensing effect generates a non-Gaussian effect due to the same gravitational potentials that produce the ISW effect at large angular scales and the lensing one at the small ones.
- The ISW-lensing bispectrum is given by:

$$b^{ISW-lensing}_{\ell_1\ell_2\ell_3} = \left\{ \frac{\ell_2(\ell_2+1) - \ell_1(\ell_1+1) - \ell_3(\ell_3+1)}{2} C^{T\psi}_{\ell_1} C^{TT}_{\ell_3} + 5\,perm \right\}$$

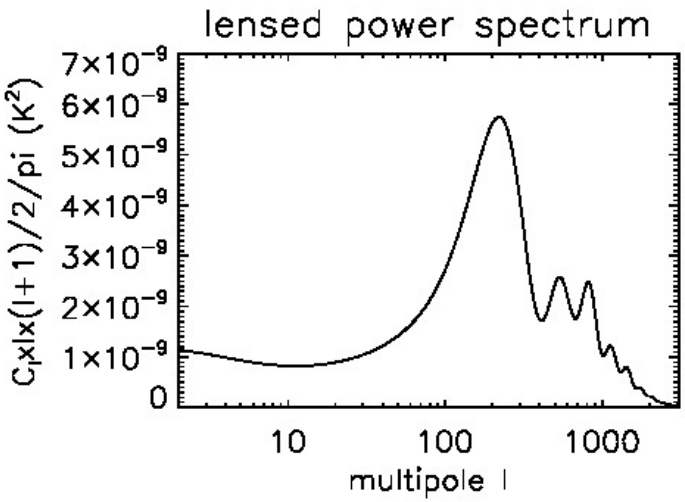

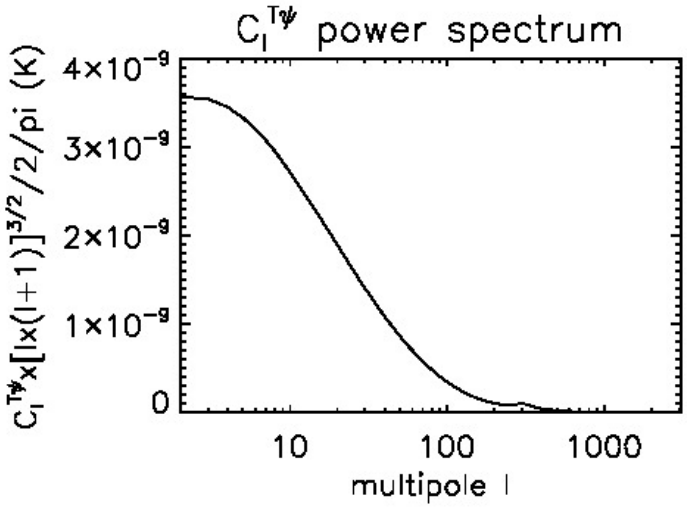

ISW-lensing and primordial bispectra

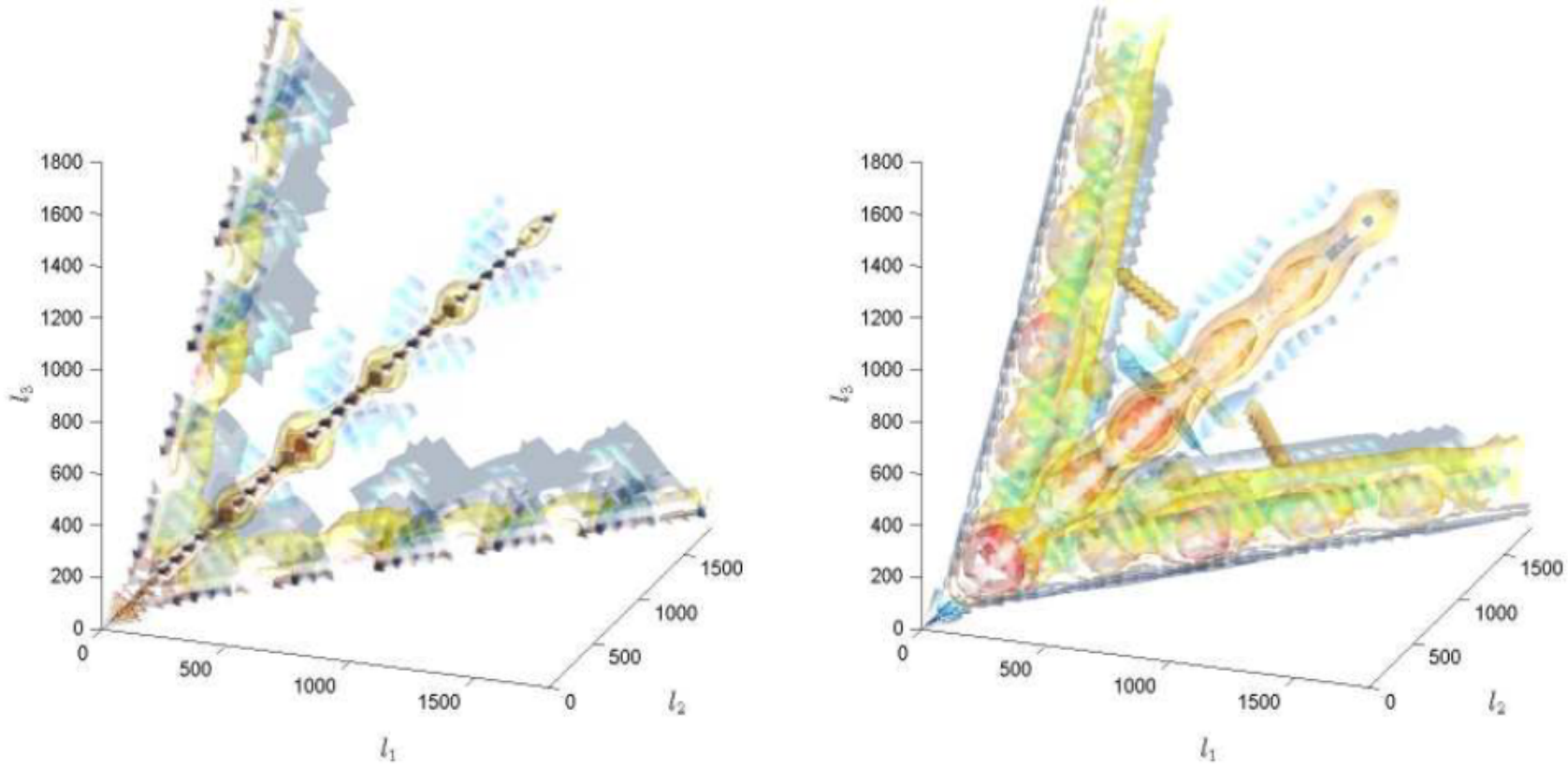

Figure 6. Contour plot of $l_1 l_2 l_3 (l_1 + l_2 + l_3) b_{l_1 l_2 l_3}$ (with non-linear intervals) for ISW-lensing (left) and local-model primordial non-Gaussianity (right; different overall scale). Although both are peaked for squeezed configurations, there are large phase and shape differences.

(from Lewis, Challinor & Hanson 2011)

Expected levels of detectability

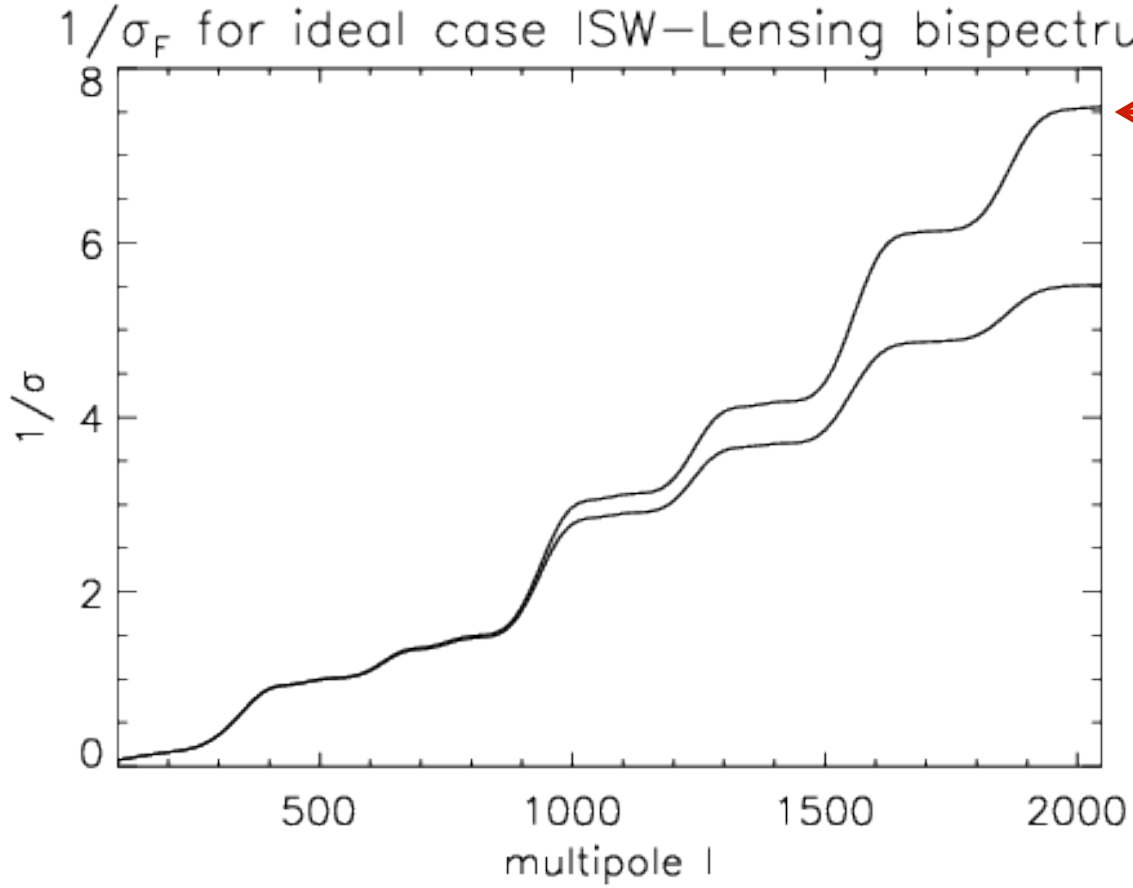

Very optimistic. Not considered the NG signal due to the ISW-lensing

Realistic. Considered the NG signal due to the ISW-lensing

See Lewis, Challinor & Hanson (2011) for more details

Expected levels of detectability

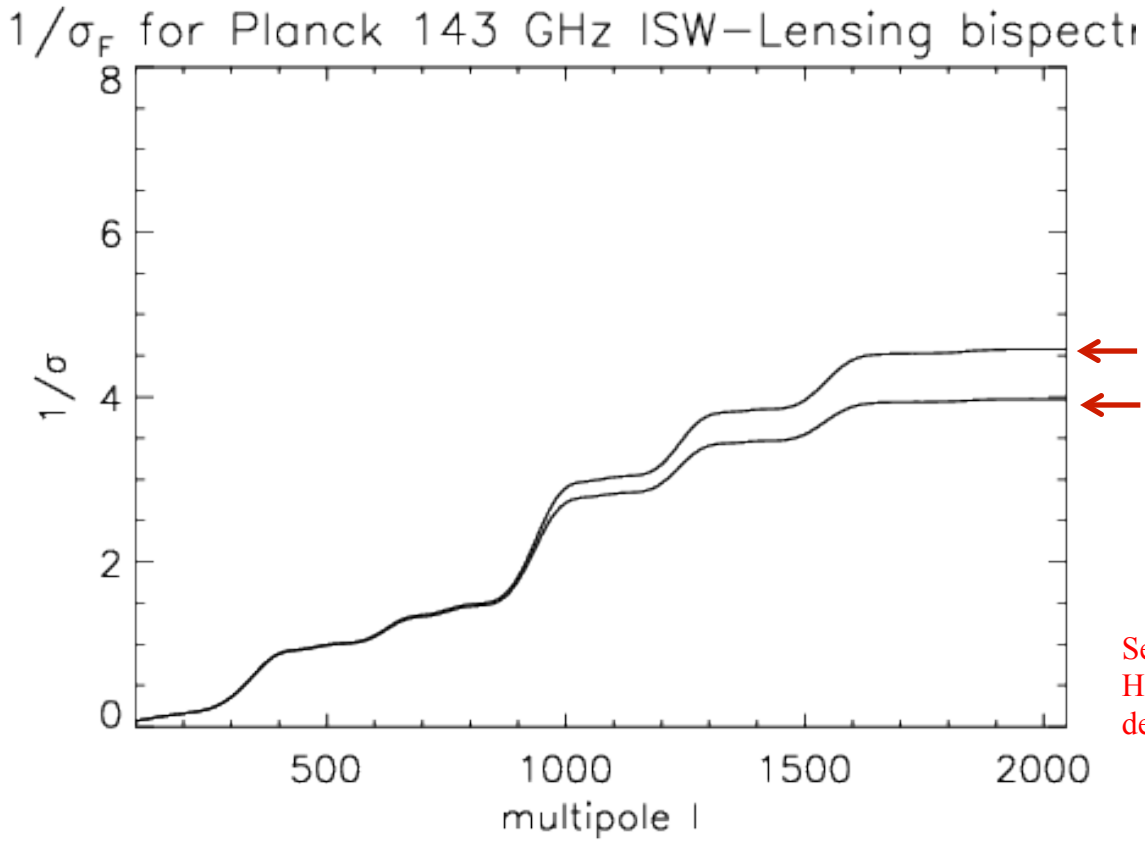

Very optimistic. Not considered the NG signal due to the ISW-lensing

Realistic. Considered the NG signal due to the ISW-lensing

See Lewis, Challinor & Hanson (2011) for more details

The sky cut also reduces this value by a factor of $\approx f_{sky}^{1/2}$.

Expected bias on local f_{nl}

$$\Delta f_{nl} = \frac{\sum_{\ell_1 \le \ell_2 \le \ell_3 \le \ell_{\max}} \frac{B^{ISW-lens}_{\ell_1\ell_2\ell_3} B^{prim}_{\ell_1\ell_2\ell_3}}{C_{\ell_1} C_{\ell_2} C_{\ell_3}}}{\sum_{\ell_1 \le \ell_2 \le \ell_3 \le \ell_{\max}} \frac{B^{prim}_{\ell_1\ell_2\ell_3} B^{prim}_{\ell_1\ell_2\ell_3}}{C_{\ell_1} C_{\ell_2} C_{\ell_3}}}$$

	$\sigma_{f_{\rm NL}}$	$\sigma_{\rm lens}$	correlation	bias on $f_{\rm NL}$	$\sigma^{\rm marge}_{f_{\rm NL}}$
T	4.31	0.19	0.24	9.5	4.44
T+E	2.14	0.12	0.022	2.6	2.14
Planck T	5.92	0.26	0.22	6.4	6.06
Planck T+E	5.19	0.22	0.13	4.3	5.23

Table 1. Errors and biases on CMB lensing and primordial local-model non-Gaussianity parameterized by $f_{\rm NL}$ for Planck-like noise (assuming isotropic coverage over the full sky with sensitivity $\Delta T = \Delta Q/2 = \Delta U/2 = 50\,\mu$K arcmin $[N_l^T = N_l^{Q/U}/4 = 2 \times 10^{-4}\mu{\rm K}^2]$ and a beam FWHM of 7 arcmin) or cosmic-variance limited data with $l_{\rm max} = 2000$. From eq. (5.35) the errors $\sigma_{f_{\rm NL}}$ and $\sigma_{\rm lens}$ are the errors on the amplitudes of the corresponding bispectrum templates individually when the other one is fixed; $\sigma^{\rm marge}_{f_{\rm NL}}$ is the Fisher error on $f_{\rm NL}$ if the amplitude of the lensing contribution is marginalized over; and the correlation is that between the two bispectrum shapes. The bias is the systematic error on $f_{\rm NL}$ if the CMB lensing contribution is neglected, i.e. eq. (5.26).

See Hanson, Smith, Challinor & Liguori (2009) and Lewis, Challinor & Hanson (2011) for more details

The ISW-lensing estimator

- The same estimators used for the primordial non-Gaussian bispectrum can be also used for the ISW-lensing one. However, the ISW-lensing signal is now significantly contributing to the bispectrum covariance matrix.
- Another approach is to first reconstruct the lensing potential ψ from the CMB temperature map and then cross-correlated with the CMB anisotropies (Lewis et al. 2011):

$$\hat{S} = \frac{1}{F}\sum_{\ell_1 m_1} C_{\ell_1}^{T\psi}\frac{\tilde{T}_{\ell_1 m_1}}{\tilde{C}_{tot,\ell_1}^{TT}}\frac{\hat{\psi}^{*}_{\ell_1 m_1}}{N_{\ell_1}^{(0)}} = \frac{1}{F}\sum_{\ell_1}(2\ell_1+1)\frac{C_{\ell_1}^{T\psi}\hat{C}_{\ell_1}^{T\psi}}{N_{\ell_1}^{(0)}}$$

$$F \approx \sum_{\ell_1}(2\ell_1+1)\left(C_{\ell_1}^{T\psi}\right)^2\left(\tilde{C}_{tot,\ell_1}^{TT}\right)^{-1}\left(N_{\ell_1}^{(0)}\right)^{-1}$$

$$\left[N_{\ell_1}^{(0)}\right]^{-1} \equiv \frac{1}{2\ell_1+1}\sum_{\ell_2\ell_3}^{\ell_1\le\ell_2\le\ell_3}\Delta_{\ell_1\ell_2\ell_3}^{-1}\frac{\left[\tilde{C}_{tot,\ell_3}^{TT}F_{\ell_2\ell_1\ell_3}^{0}+\tilde{C}_{tot,\ell_2}^{TT}F_{\ell_3\ell_1\ell_2}^{0}\right]^2}{\tilde{C}_{tot,\ell_2}^{TT}\tilde{C}_{tot,\ell_3}^{TT}}$$

Cubic statistics for ISW-lensing bispectrum

- Select a characteristic set of angular scales R_j
- Compute the wavelet transform map $w(b_i,R_j)$ at these scales R_j
- Compute third order statistics by combining different scales

$$q_{ijk} = \frac{1}{\sigma_i \sigma_j \sigma_k} \int w(\vec{b}, R_i) w(\vec{b}, R_j) w(\vec{b}, R_k) d\vec{b}$$

Arxiv:1007.2181

- Combine in a χ^2 test all the estimators

$$\chi^2(A) = \sum_{ijk,rst} (q_{ijk} - \langle q_{ijk} \rangle_A) C^{-1}_{ijk,rst}(A) (q_{rst} - \langle q_{rst} \rangle_A)$$

data

ISW-lensing model

Because there is guaranteed non-Gaussian signal present due to the ISW-lensing, the covariance is larger and it should be computed as a function of A (See Lewis et al 2011)

Point source contaminants

- Two main populations:
  - Extragalactic radio sources
  - Infra-red extragalactic sources

Extragalactic Radio Sources

- At mm and sub-mm wavelengths, radio sources are dominated by **blazars** (AGN-powered sources with flat spectrum at GHz frequencies)

- Blazar spectra bend to **steeper laws** starting from few tens (e.g., ATCA, Planck, etc.)

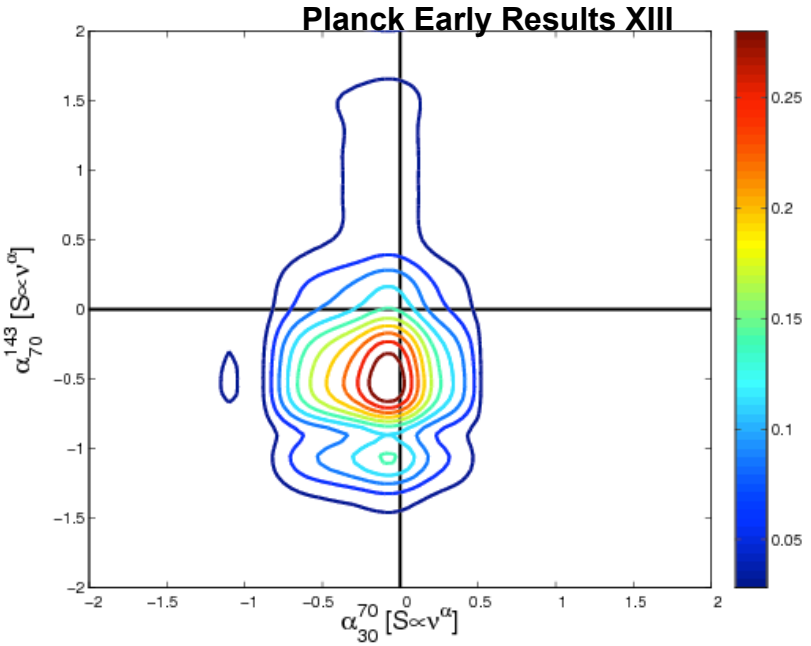

- High-frequency number counts are well described by the **Tucci et al. (2011) model**: it introduces a break in blazar spectra, as predicted by classical physical models for the synchrotron emission in AGN jets.

Polarization of Extragalactic Radio Sources

The typical linear polarization degree (Π) is **few per cent**, indication of a low order of magnetic fields.

- For **Blazars** median Π is 2-3% [1,10]GHz; 3-3.5% [10,40]GHz; maybe higher at v>40GHz (Battye+2011; Agudo+2010)

- From available data, no clear dependence of fractional polarization with flux density

Values used in the analysis (Tucci&Toffolatti12):

	Π_{med}	$\langle\Pi^2\rangle^{1/2}$
Steep	4%	6%
FSRQ	3%	3.8%
BLLac	3.6%	4.5%

Tucci&Toffolatti 2012

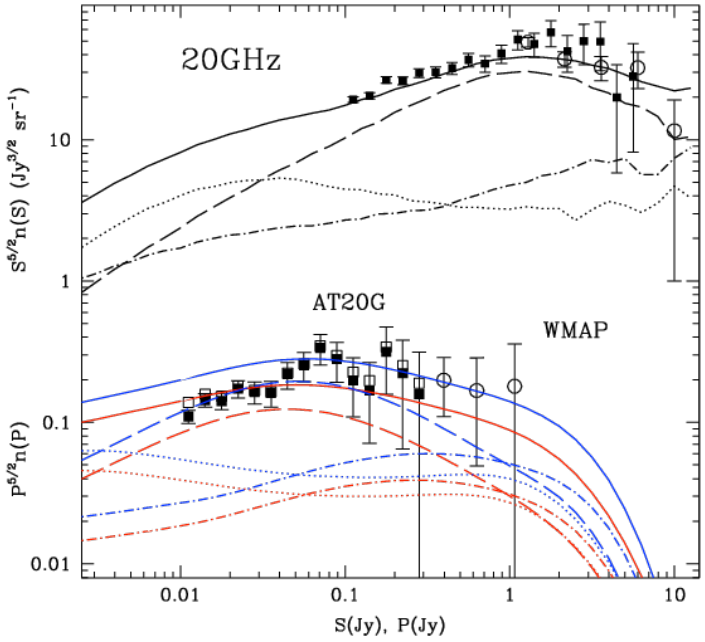

Infra-red Extragalactic sources

- Bright sources (Jy or sub-Jy level): spiral or starburst galaxies at low z
- At mJy level, powerful high-z galaxies (z>1). These are interpreted as massive proto-spheroidal galaxies in the process of forming most of their stellar mass (e.g., Lapi et al. 2011).
- Significant number of high-z galaxies can undergo to a magnification of flux density by gravitational lensing

- Star-forming proto-spheroidal galaxies account for a substantial fraction of the CIB (increasingly at higher wavelengths)

Polarization of IR galaxies:
very few information, typically taken
Π=1%

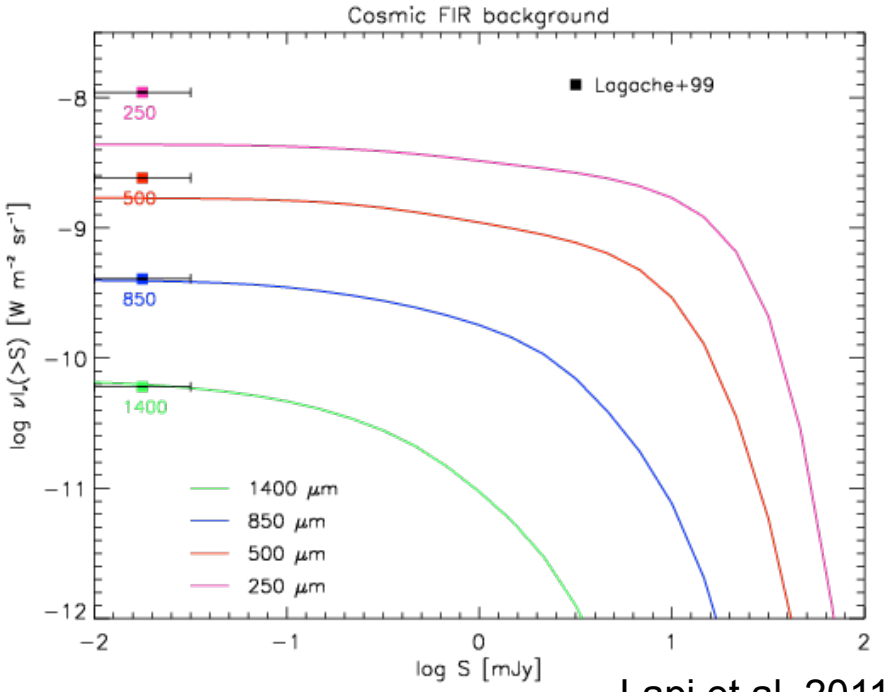

Lapi et al. 2011

Number Counts of Extragalactic Sources

150 GHz

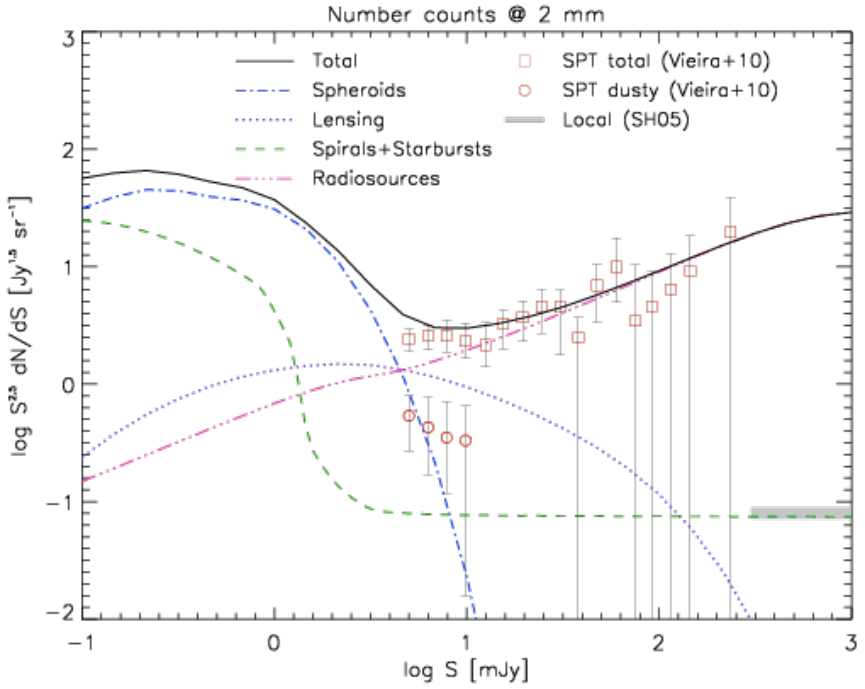

220 GHz

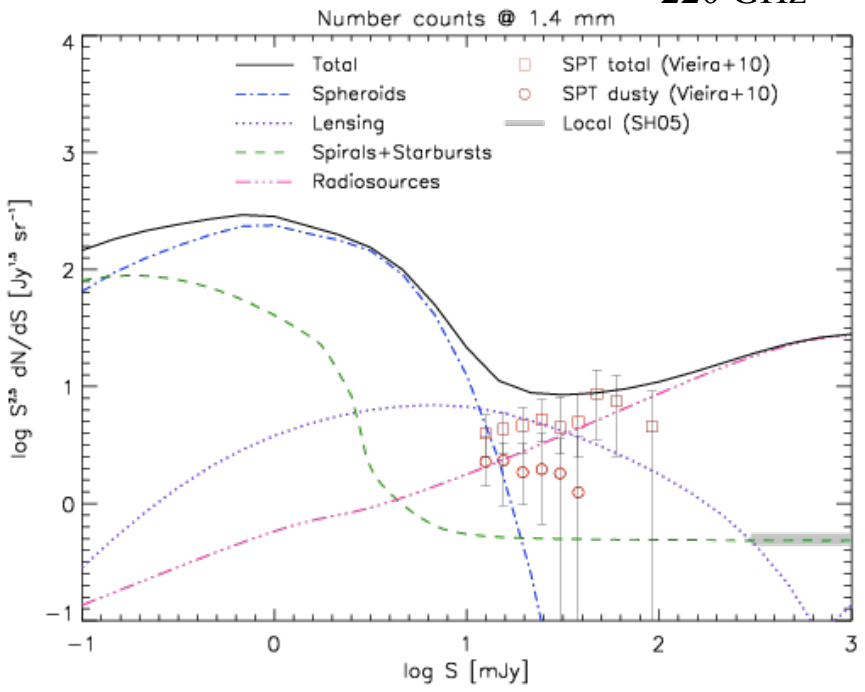

Lapi et al. 2011

Power Spectra from Poisson distributed Point Sources

- **Temperature PS**

$$C_{T\ell} = \left(\frac{dB}{dT}\right)^2 N\left\langle S^2 \right\rangle = \left(\frac{dB}{dT}\right)^2 \int n(S) S^2 dS$$

- **Polarization PS**

$$C_{Q\ell} \approx C_{U\ell} \approx C_{E\ell} \approx C_{B\ell}$$

$$C_{Q\ell} = \left(\frac{dB}{dT}\right)^2 N\left\langle Q^2 \right\rangle = \left(\frac{dB}{dT}\right)^2 N\left\langle S^2 \Pi^2 \cos^2(2\varphi) \right\rangle = \frac{1}{2}\left\langle \Pi^2 \right\rangle C_{T\ell}$$

- **Cross PS (Temperature-Polarization)**

$$C_{TQ\ell} = \left(\frac{dB}{dT}\right)^2 \left\langle S^2 \Pi \cos(2\varphi) \right\rangle = 0$$

Power spectrum of spatially correlated sources, see Argüeso et al (2003)

Extragalactic Sources vs CMB T Power Spectrum

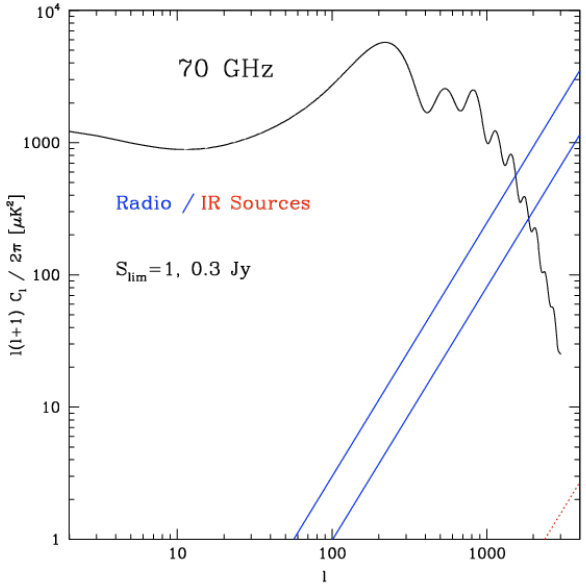

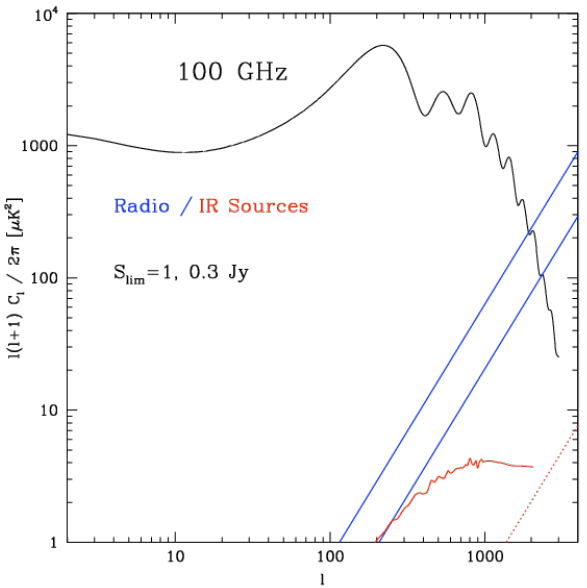

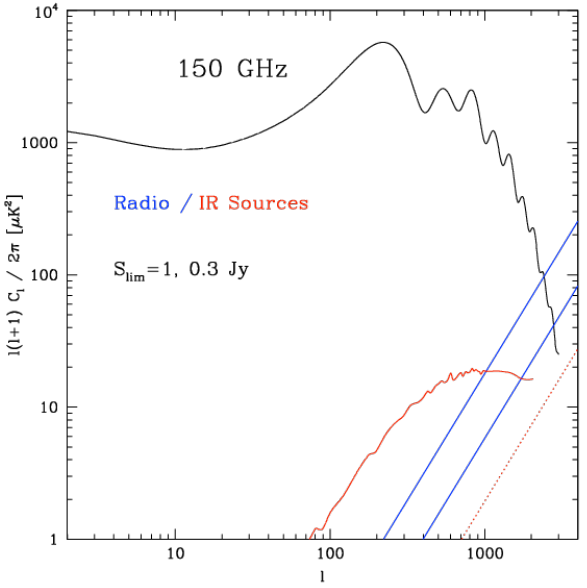

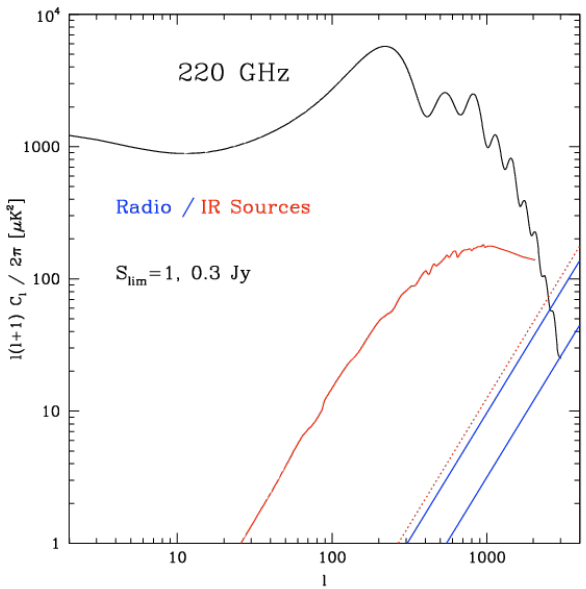

E- and B-mode Power Spectra

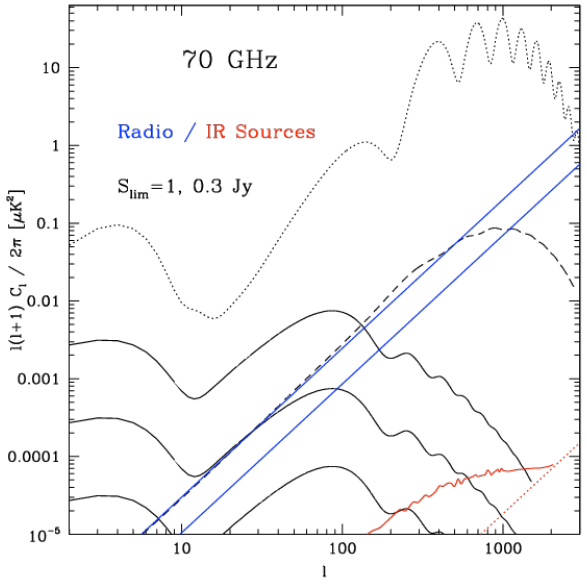

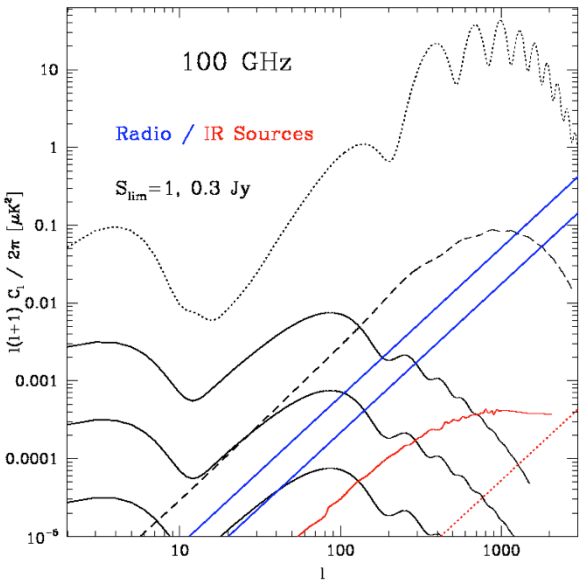

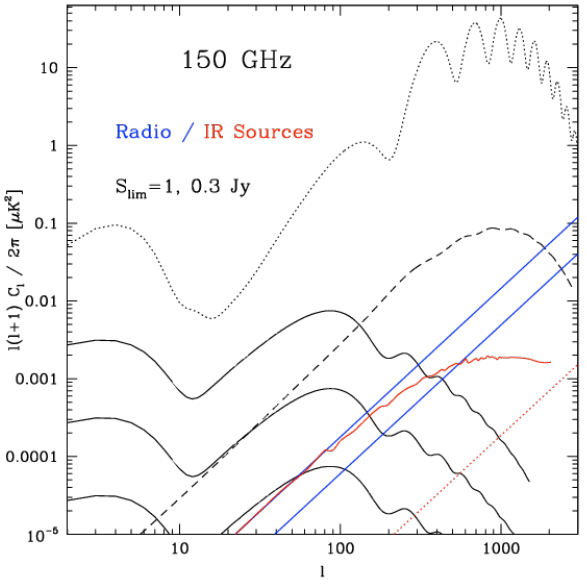

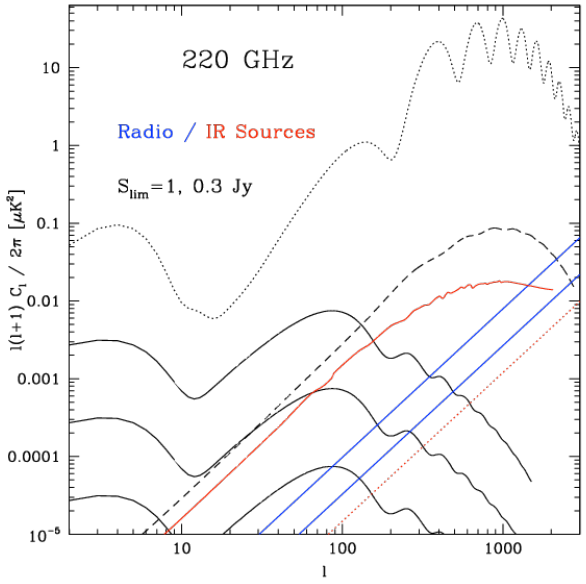

Characteristic selection of COrE parameters

Freq (GHz)	45	75	105	165	225	375
Beam FWHM	23.3	14.0	10.0	6.4	4.7	2.8
Temp: σ_{noise} (μK·arcmin)	5.25	2.73	2.68	2.67	2.64	68.6
Pol: σ_{noise} (μK·arcmin)	9.07	4.72	4.63	4.61	4.57	119

Parameters from COrE white paper http://arxiv.org/abs/1102.2181

- Considered two flux limits for each frequency:

  S_{lim} = 0.3 Jy
  S_{lim} = 1 Jy

- Maximum multipole l_{max} = 2048
- Considered cases:
  Ideal conditions
  COrE instrumental conditions

The sources

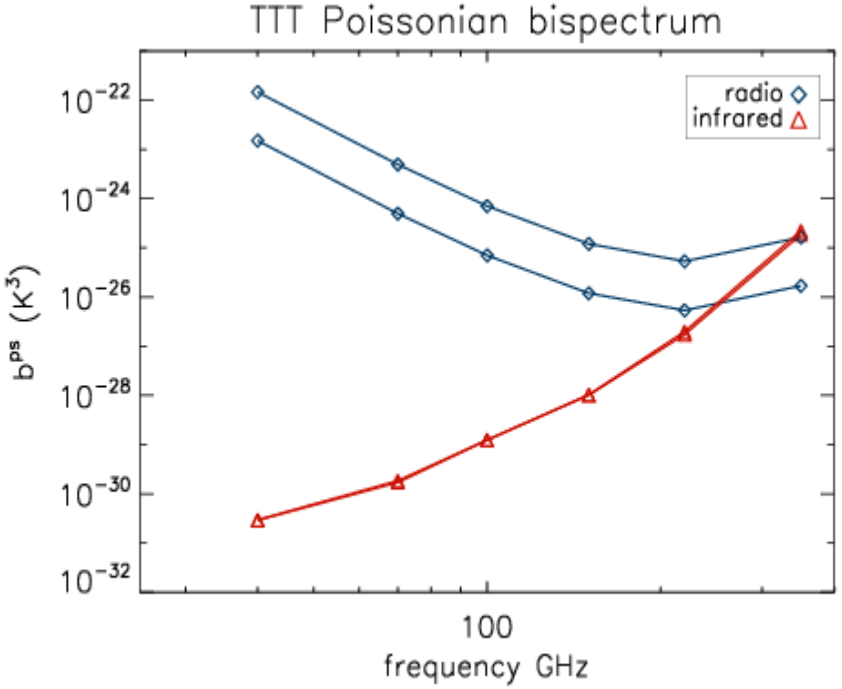

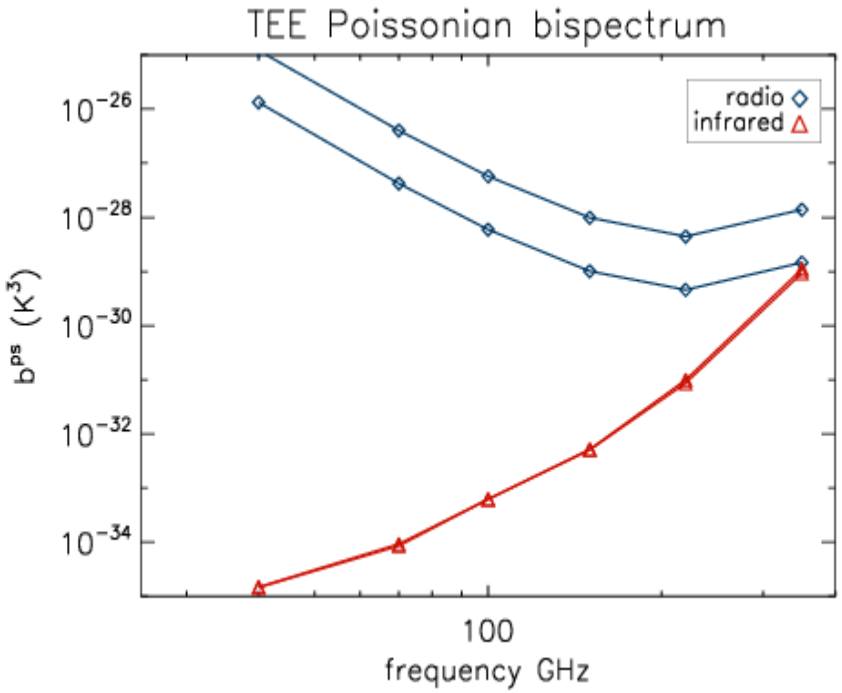

Top lines: S_c = 1 Jy Bottom lines: S_c = 0.3 Jy

$$B^{PS}_{\ell_1\ell_2\ell_3} = B^{radio} + B^{ir,poiss}\sqrt{\frac{C^{ir}_{\ell_1}C^{ir}_{\ell_2}C^{ir}_{\ell_3}}{C^{ir,poiss}_{\ell_1}C^{ir,poiss}_{\ell_2}C^{ir,poiss}_{\ell_3}}}$$

Contamination in primordial non-Gaussianity (f_{nl})

Curto et al (2012), in preparation

Primordial non-Gaussianity f_{nl} bias estimator (T)

$$\Delta f_{nl} = \frac{\sum_{\ell_1 \le \ell_2 \le \ell_3 \le \ell_{\max}} \frac{B^{ps}_{\ell_1\ell_2\ell_3} B^{prim}_{\ell_1\ell_2\ell_3}}{\Delta_{\ell_1\ell_2\ell_3} C_{\ell_1} C_{\ell_2} C_{\ell_3}}}{\sum_{\ell_1 \le \ell_2 \le \ell_3 \le \ell_{\max}} \frac{B^{prim}_{\ell_1\ell_2\ell_3} B^{prim}_{\ell_1\ell_2\ell_3}}{\Delta_{\ell_1\ell_2\ell_3} C_{\ell_1} C_{\ell_2} C_{\ell_3}}}$$

$$\sigma^2\left(f_{nl}\right) = \frac{1}{\sum_{\ell_1 \le \ell_2 \le \ell_3 \le \ell_{\max}} \frac{B^{prim}_{\ell_1\ell_2\ell_3} B^{prim}_{\ell_1\ell_2\ell_3}}{\Delta_{\ell_1\ell_2\ell_3} C_{\ell_1} C_{\ell_2} C_{\ell_3}}}$$

Total power spectrum

$$C_\ell = \left(C_\ell^{CMB} + C_\ell^{IR\,PS} + C_\ell^{Radio\,PS}\right) b_\ell^2 w_\ell^2 + C_\ell^{noise}$$

CMB power spectrum

Infra-red point source power spectrum

radio point source power spectrum

Instrumental noise

Primordial non-Gaussianity f_{nl} bias estimator (T and E)

$$\Delta f_{nl} = \frac{\sum_{ijk,rst,\ell_1 \le \ell_2 \le \ell_3 \le \ell_{\max}} B^{ijk,ps}_{\ell_1\ell_2\ell_3} C^{-1}_{ijk,rst} B^{rst,prim}_{\ell_1\ell_2\ell_3}}{\sum_{ijk,rst,\ell_1 \le \ell_2 \le \ell_3 \le \ell_{\max}} B^{ijk,prim}_{\ell_1\ell_2\ell_3} C^{-1}_{ijk,rst} B^{rst,prim}_{\ell_1\ell_2\ell_3}}$$

$$\sigma^2\left(f_{nl}\right) = \frac{1}{\sum_{ijk,rst,\ell_1 \le \ell_2 \le \ell_3 \le \ell_{\max}} B^{prim}_{\ell_1\ell_2\ell_3} C^{-1}_{ijk,rst} B^{prim}_{\ell_1\ell_2\ell_3}}$$

Indices i, j, k, r, s, t = {T, E}

Power spectrum covariance

$$C_{ijk,pqr} = C^{ip}_{\ell_1} C^{jq}_{\ell_2} C^{kr}_{\ell_3} + C^{ip}_{\ell_1} C^{jr}_{\ell_2} C^{kq}_{\ell_3} \delta_{\ell_2\ell_3} + C^{ir}_{\ell_1} C^{jq}_{\ell_2} C^{kp}_{\ell_3} \delta_{\ell_1\ell_3} + C^{iq}_{\ell_1} C^{jp}_{\ell_2} C^{kr}_{\ell_3} \delta_{\ell_1\ell_2} + \\ + C^{iq}_{\ell_1} C^{jr}_{\ell_2} C^{kp}_{\ell_3} \delta_{\ell_1\ell_2} \delta_{\ell_2\ell_3} \delta_{\ell_1\ell_3} + C^{ir}_{\ell_1} C^{jp}_{\ell_2} C^{kq}_{\ell_3} \delta_{\ell_1\ell_3} \delta_{\ell_2\ell_1} \delta_{\ell_2\ell_3}$$

Polarization non-zero point source power spectrum and bispectrum (even number of E)

$$b^{TEE} = \left\langle p^2 \right\rangle \left\langle \cos^2(2\phi) \right\rangle b^{TTT} \qquad b^{TTE} = b^{EEE} = 0$$

Ideal conditions

Full sky, no beam nor instrumental noise considered

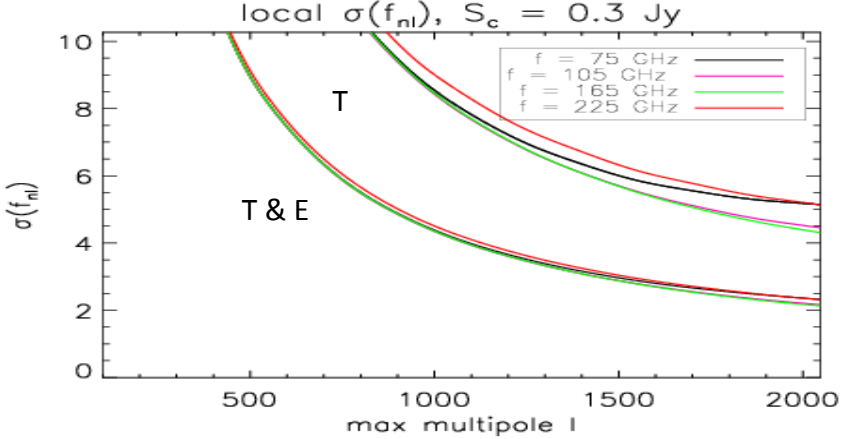
local σ(f_nl), S_c = 0.3 Jy
f = 75 GHz
f = 105 GHz
f = 165 GHz
f = 225 GHz
T
T & E
σ(f_nl)
max multipole l

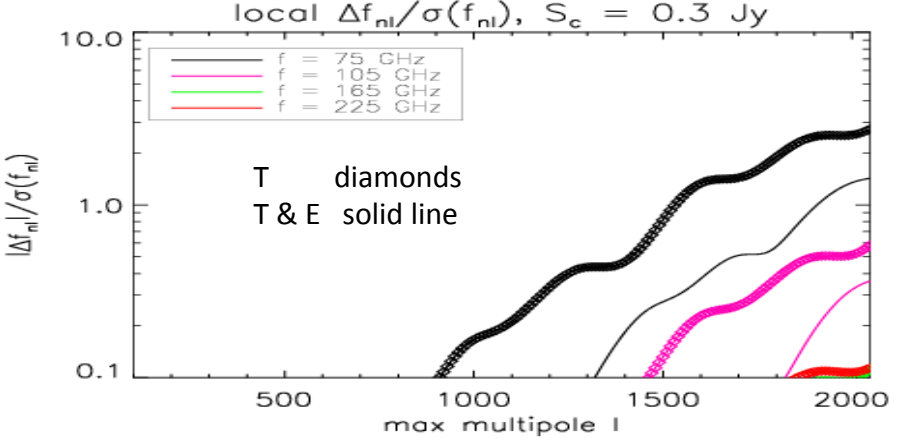
local Δf_nl/σ(f_nl), S_c = 0.3 Jy
f = 75 GHz
f = 105 GHz
f = 165 GHz
f = 225 GHz
T diamonds
T & E solid line
|Δf_nl|/σ(f_nl)
max multipole l

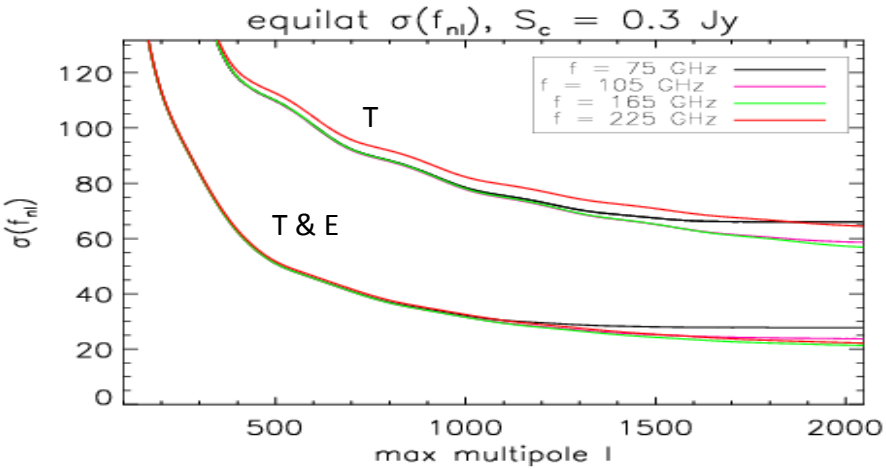
equilat σ(f_nl), S_c = 0.3 Jy
f = 75 GHz
f = 105 GHz
f = 165 GHz
f = 225 GHz
T
T & E
σ(f_nl)
max multipole l

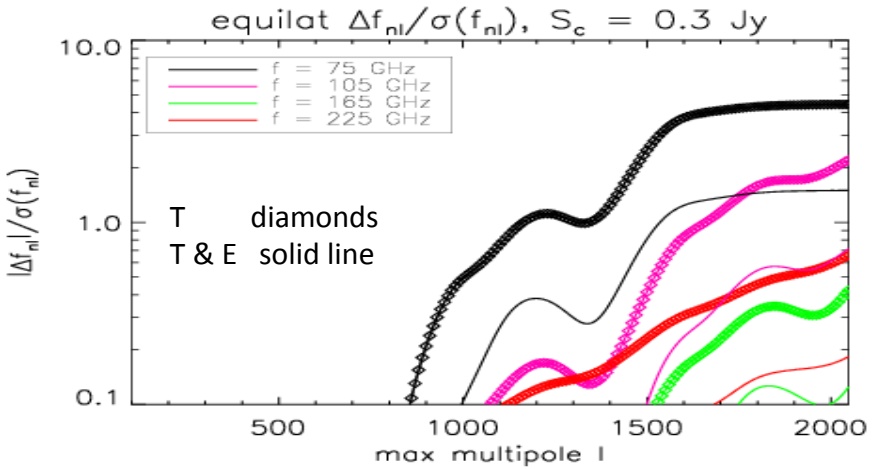
equilat Δf_nl/σ(f_nl), S_c = 0.3 Jy
f = 75 GHz
f = 105 GHz
f = 165 GHz
f = 225 GHz
T diamonds
T & E solid line
|Δf_nl|/σ(f_nl)
max multipole l

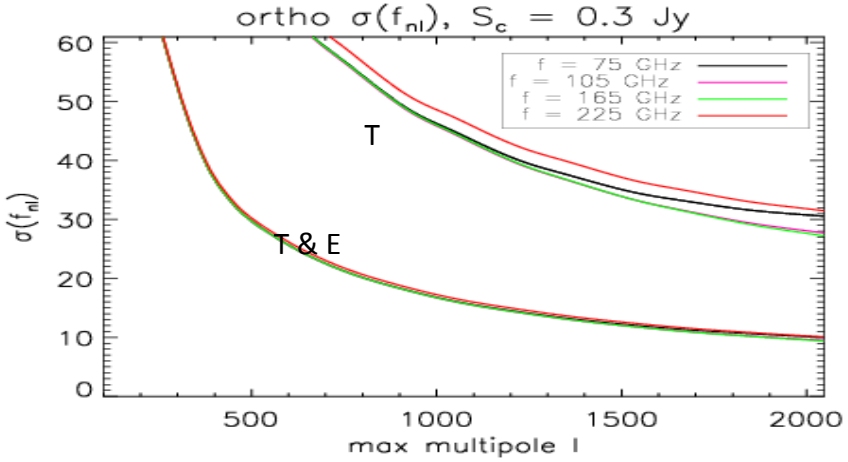
ortho σ(f_nl), S_c = 0.3 Jy
f = 75 GHz
f = 105 GHz
f = 165 GHz
f = 225 GHz
T
T & E
σ(f_nl)
max multipole l

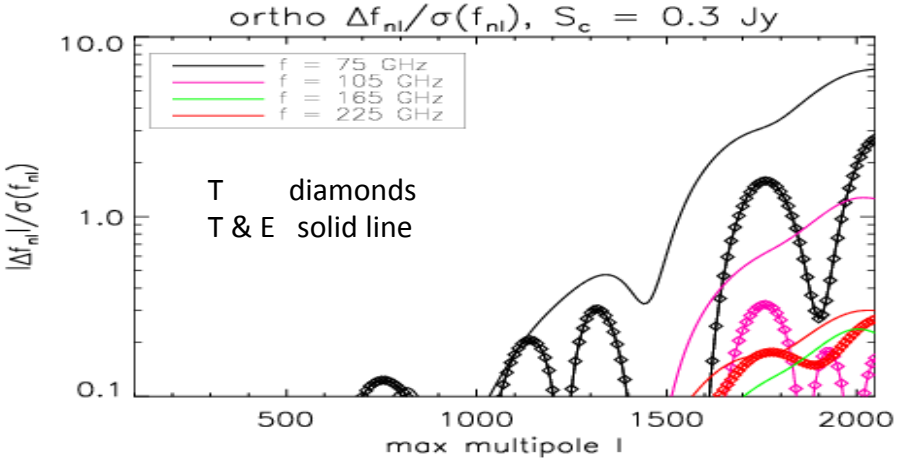
ortho Δf_nl/σ(f_nl), S_c = 0.3 Jy
f = 75 GHz
f = 105 GHz
f = 165 GHz
f = 225 GHz
T diamonds
T & E solid line
|Δf_nl|/σ(f_nl)
max multipole l

Predictions for COrE maps

Full sky, beam and instrumental noise considered

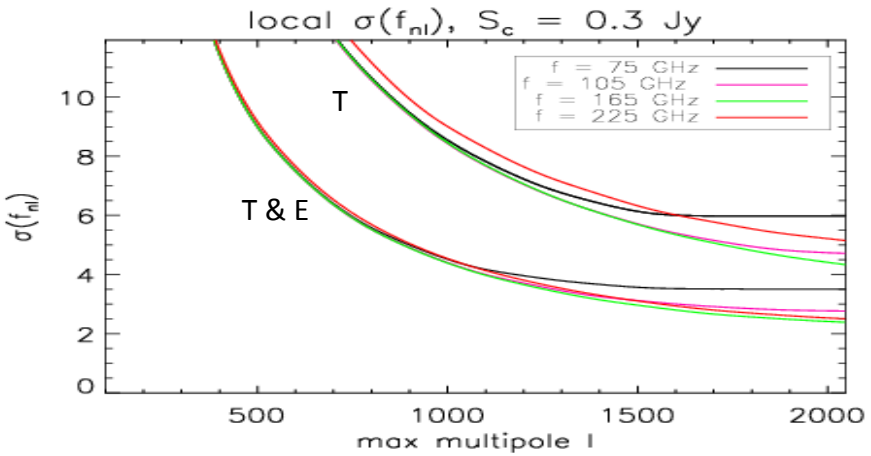
local σ(f_nl), S_c = 0.3 Jy
f = 75 GHz
f = 105 GHz
f = 165 GHz
f = 225 GHz
T
T & E
σ(f_nl)
max multipole l

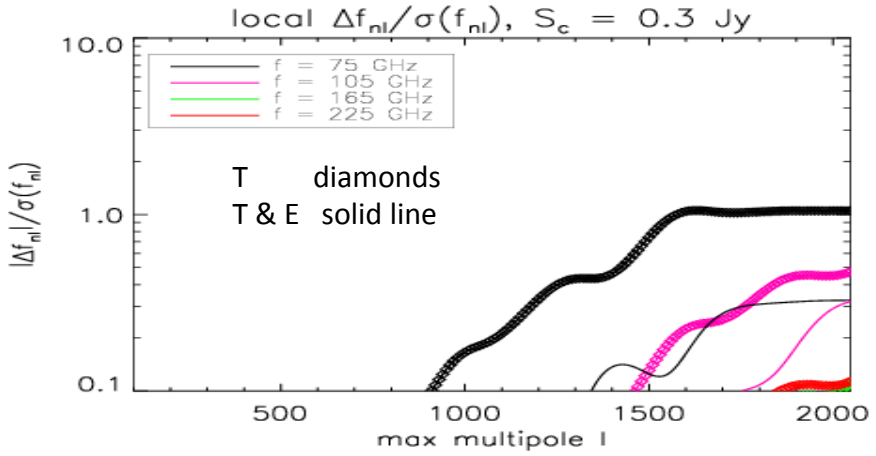
local Δf_nl/σ(f_nl), S_c = 0.3 Jy
f = 75 GHz
f = 105 GHz
f = 165 GHz
f = 225 GHz
T diamonds
T & E solid line
|Δf_nl|/σ(f_nl)
max multipole l

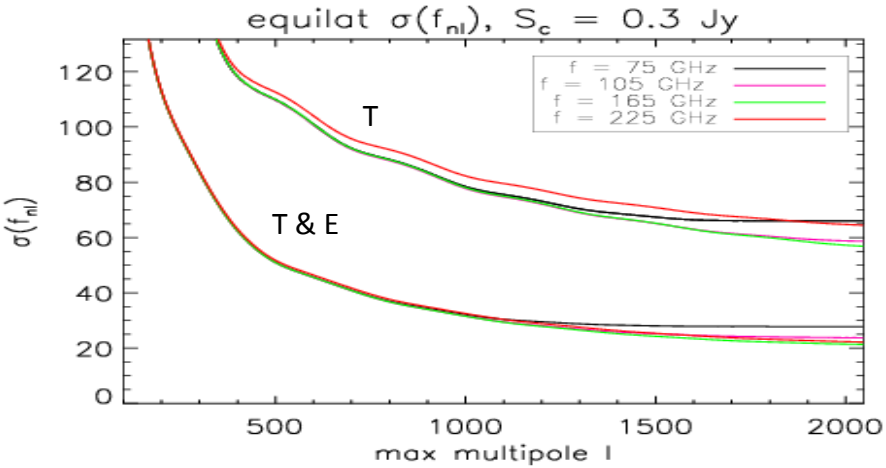
equilat σ(f_nl), S_c = 0.3 Jy
f = 75 GHz
f = 105 GHz
f = 165 GHz
f = 225 GHz
T
T & E
σ(f_nl)
max multipole l

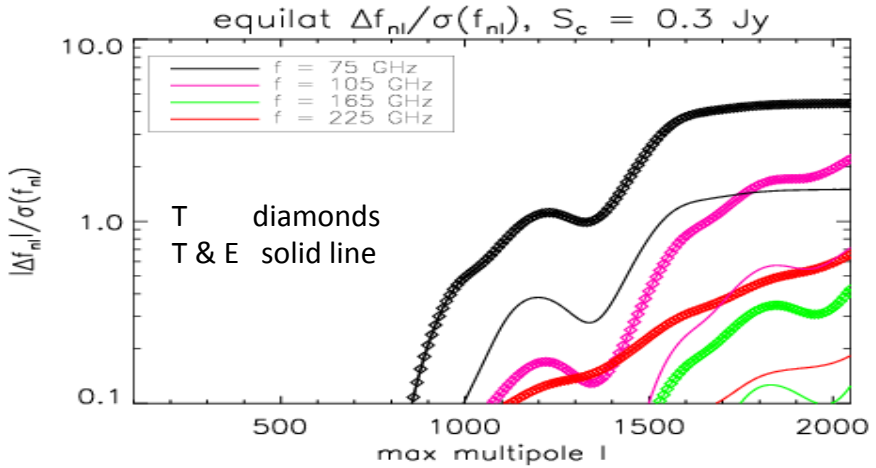
equilat Δf_nl/σ(f_nl), S_c = 0.3 Jy
f = 75 GHz
f = 105 GHz
f = 165 GHz
f = 225 GHz
T diamonds
T & E solid line
|Δf_nl|/σ(f_nl)
max multipole l

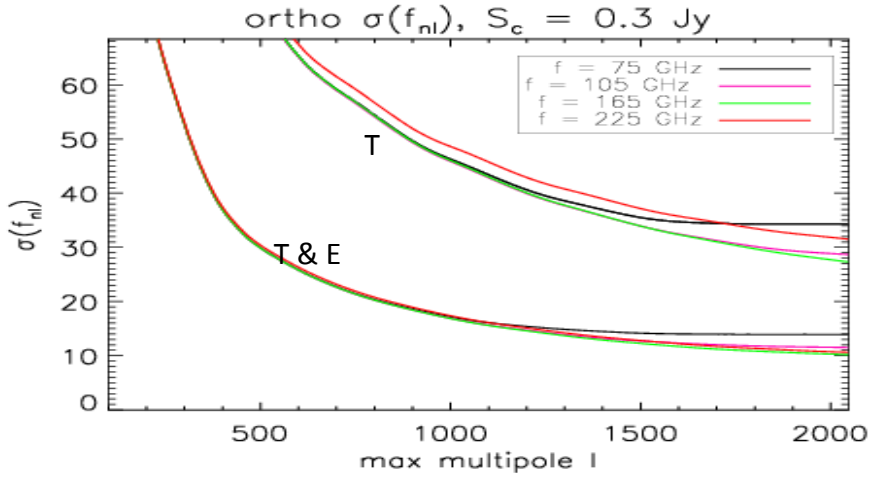
ortho σ(f_nl), S_c = 0.3 Jy
f = 75 GHz
f = 105 GHz
f = 165 GHz
f = 225 GHz
T
T & E
σ(f_nl)
max multipole l

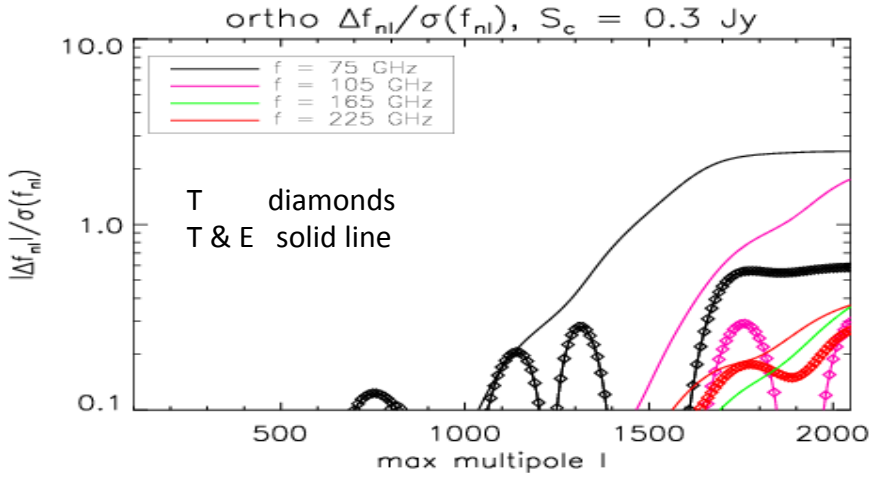
ortho Δf_nl/σ(f_nl), S_c = 0.3 Jy
f = 75 GHz
f = 105 GHz
f = 165 GHz
f = 225 GHz
T diamonds
T & E solid line
|Δf_nl|/σ(f_nl)
max multipole l

Summary for local shape

Ideal, S_c = 0.3 Jy

f	45	75	105	165	225	375
Δf_{nl}	118.9	14.1	2.6	0.5	0.6	18.6
$\sigma(f_{nl})$	8.4	5.1	4.4	4.3	5.1	19.4
Δf_{nl}	-8.7	-3.3	-0.8	-0.2	-0.1	-0.3
$\sigma(f_{nl})$	2.9	2.3	2.2	2.1	2.3	3.1

COrE, S_c = 0.3 Jy

f	45	75	105	165	225	375
Δf_{nl}	31.4	6.3	2.2	0.5	0.6	17.9
$\sigma(f_{nl})$	10.2	6.0	4.7	4.3	5.1	19.6
Δf_{nl}	3.7	-1.1	-0.9	-0.2	-0.2	7.6
$\sigma(f_{nl})$	6.2	3.5	2.8	2.4	2.5	15.3

Ideal, S_c = 1 Jy

f	45	75	105	165	225	375
Δf_{nl}	470.8	88.6	21.5	4.4	2.1	19.0
$\sigma(f_{nl})$	11.5	6.3	5.0	4.5	5.2	19.5
Δf_{nl}	22.3	-14.9	-5.2	-1.3	-0.5	-0.3
$\sigma(f_{nl})$	3.5	2.5	2.3	2.2	2.3	3.1

COrE, S_c = 1 Jy

f	45	75	105	165	225	375
Δf_{nl}	232.5	51.7	19.1	4.4	2.1	18.3
$\sigma(f_{nl})$	12.4	6.7	5.1	4.5	5.2	19.7
Δf_{nl}	28.4	-9.8	-7.4	-1.6	-0.5	7.7
$\sigma(f_{nl})$	7.1	3.8	2.9	2.4	2.5	15.4

T

T & E

Summary for equilateral shape

Ideal, S_c = 0.3 Jy

f	45	75	105	165	225	375
Δf_{nl}	6400	835.9	137.0	23.8	42.5	804.2
$\sigma(f_{nl})$	81.1	61.6	57.3	56.8	64.3	164.5
Δf_{nl}	720.9	77.7	10.0	1.3	3.5	23.1
$\sigma(f_{nl})$	25.6	20.6	19.6	19.4	20.9	32.1

COrE, S_c = 0.3 Jy

f	45	75	105	165	225	375
Δf_{nl}	824.4	293.1	129.1	24.1	42.5	775.6
$\sigma(f_{nl})$	87.3	65.9	58.5	56.7	64.3	164.9
Δf_{nl}	126.8	41.5	16.9	2.6	4.0	351.7
$\sigma(f_{nl})$	42.1	27.7	23.6	21.1	22.0	114.9

Ideal, S_c = 1 Jy

f	45	75	105	165	225	375
Δf_{nl}	21930	5224	1255	234.1	126.2	819.4
$\sigma(f_{nl})$	96.9	68.6	60.7	57.8	64.8	164.6
Δf_{nl}	3256	505.7	113.8	16.9	9.9	25.2
$\sigma(f_{nl})$	30.2	22.3	20.4	19.7	21.0	32.2

COrE, S_c = 1 Jy

f	45	75	105	165	225	375
Δf_{nl}	6098	2408	1129	234.7	126.1	789.9
$\sigma(f_{nl})$	98.9	70.4	61.3	57.9	64.9	165.0
Δf_{nl}	889.7	319.8	143.4	26.4	11.7	358.8
$\sigma(f_{nl})$	45.9	28.7	24.2	21.4	22.1	115.1

T

T & E

Summary for orthogonal shape

Ideal, S_c = 0.3 Jy

f	45	75	105	165	225	375
Δf_{nl}	1597	83.2	4.5	0.2	8.5	335.8
$\sigma(f_{nl})$	44.3	30.5	27.7	27.2	31.4	98.8
Δf_{nl}	401.5	65.8	11.9	2.1	3.1	11.8
$\sigma(f_{nl})$	12.4	9.9	9.4	9.3	10.0	15.1

COrE, S_c = 0.3 Jy

f	45	75	105	165	225	375
Δf_{nl}	97.2	20.1	8.6	0.3	8.5	327.9
$\sigma(f_{nl})$	51.7	34.2	28.6	27.2	31.4	99.3
Δf_{nl}	24.2	34.5	19.8	3.6	3.9	138.4
$\sigma(f_{nl})$	22.3	13.9	11.4	10.1	10.6	62.9

Ideal, S_c = 1 Jy

f	45	75	105	165	225	375
Δf_{nl}	7977	815.2	110.7	8.1	14.3	342.3
$\sigma(f_{nl})$	56.7	35.2	29.8	27.9	31.8	99.2
Δf_{nl}	1128	372.2	99.6	19.8	8.9	12.0
$\sigma(f_{nl})$	14.7	10.7	9.8	9.5	10.1	15.1

COrE, S_c = 1 Jy

f	45	75	105	165	225	375
Δf_{nl}	1342	254.5	104.8	8.9	14.3	334.4
$\sigma(f_{nl})$	60.1	37.2	30.4	28.0	31.8	99.6
Δf_{nl}	204.7	279.9	166.5	32.6	11.7	141.0
$\sigma(f_{nl})$	24.7	14.5	11.8	10.3	10.6	63.1

T

T & E

Summary of the point source contamination

- Power spectrum:
  - Temperature: contamination of radio sources is mostly located at multipoles l > 2000
  - Significant contamination for the cosmological B mode at all frequencies if $r < 10^{-2}$
  - The IR sources are not highly dependent to the S_c
- Bispectrum:
  - B_{PS} is zero for odd polarization combinations
  - Radio B_{PS} larger than IR B_{PS} for $\nu <= 200$ GHz (both TTT and TEE)
- Non-Gaussianity f_{nl} bias:
  - The polarization reduces the bias and the $\sigma(f_{nl})$ on all the considered f_{nl} shapes
  - Negligible bias contamination for $150 < \nu < 225$ GHz

Summary

- Non-Gaussianity studies represent an important complement to the power spectrum to constrain inflationary models.
- Optimal estimators of f_{NL} are implemented in different spaces (harmonic, wavelets, modal). They are an important test to check for systematics and foreground contamination.
- The ISW-lensing bispectrum is expected to be detected at the 3-4σ with Planck. It also produces a bias in the local primordial shape of Δf_{NL}=7-9
- The extragalactic point sources bias the value of f_{NL} by a relatively small amount (smaller than the expected error bar for each shape). Including polarization the bias is decreased.
- When estimating f_{NL} all possible contributions should be considered (primordial, ISW-lensing, extragalactic point sources, Galactic foregrounds).
- Planck is expected to improve WMAP results on f_{NL} by a factor of approx. 5.